Utrecht University

Realistic terrain features and the complexity of joint viewsheds

Gert G.T. Meijer

Master Thesis
ICA-6026087

Game and Media Technology
Department of Information and Computing Sciences
Utrecht University

Supervised by:
dr. Maarten Löffler
dr. Frank Staals
dr. Rodrigo I. Silveira

August 25, 2020

Acknowledgements

I would like to thank my supervisors, Maarten, Frank, and Rodrigo, for their time, valuable insight, and for including me in their research. Our regular meetings were a welcome consistency during the project and provided me with many ideas to work with. I am especially thankful for the flexibility of my supervisors and the department around the format and location of this master thesis.

I would also like to thank my family and friends who have always believed in me throughout my many years of study, giving me the drive to never give up. Also, their understanding of my lack of time during the last year is greatly appreciated.

Abstract

Computing viewsheds from different viewpoints is an important procedure with many applications in multiple Geographic Information Science (GIS) fields. While much research has been done on viewsheds obtained from a single viewpoint, viewsheds from multiple viewpoints are still mostly unexplored. This thesis attempts to give more insight into the complexity of multiple viewsheds by analyzing several measures from different GIS fields on real-world terrains. *Sky visibility index, terrain ruggedness index, terrain shape index, fractal Dimension*, and *prickliness* were calculated on datasets of around 50 real-world terrains and statistically analyzed with viewsheds generated from multiple viewpoint configurations. Because GIS fields have different preferences on terrain representations, both *digital elevation model* (DEM) and *triangular irregular network* (TIN) terrains were used. This thesis shows some relevant insight into the behavior of viewsheds on realistic terrains. It also provides evidence that measures like *prickliness* are a good indicator for (multiple) viewshed complexity in some common use cases.

Contents

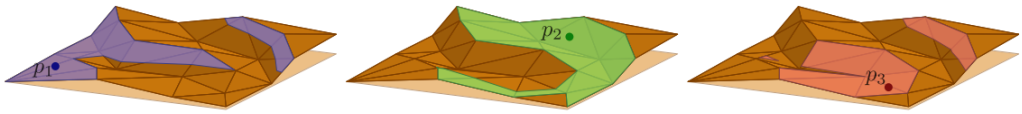

Fig. 1: The viewsheds of three viewpoints on a 2.5D terrain. (From Hurtado et al. [1])

1 Introduction

Visibility is an important topic within multiple fields; examples of problems include finding the best locations to place cameras, determining visible geometry within a 3D environment (e.g., in games), and guard (tower) placement [2]. Visibility is not limited to sight problems, for example, finding the best locations to place radio towers [3] or Wi-Fi hotspots can also be seen as visibility problems. Within the geosciences visibility tools are used for the analysis of archaeological locations and urban environment planning [4, 5]. In essence, all these problems pose the same question: *"Amidst several obstacles, are two points visible from each other?"* The focus of this thesis is on 2.5D terrains. In other words, xy-monotone surfaces in $\mathbb{R}^3$, meaning any vertical line intersects the surface at most once. An important concept related to visibility is the *viewshed* of one or multiple viewpoints. A viewshed is defined as the regions of a terrain that are visible from the viewpoint, see Figure 1. Within this thesis, viewpoints are assumed to have unlimited sight distance.

The computation of a viewshed belonging to a single viewpoint is a well-studied topic. However, Hurtado *et al.* [1] found that the problem of computing the viewshed (or *visibility map*) belonging to multiple viewpoints had been left open. They studied visibility maps on 1.5D and 2.5D terrains, introduce three visibility structures, and analyze their space and time complexities for both dimensions. For 2.5D terrains, they show that the visibility map can have $\Omega(m^2n^2)$ complexity. This is proven using a theoretical *"courtyard"* terrain, see Figure 2. However, in the real world, this type of terrain is not commonly encountered. Therefore, it is interesting to explore the complexity of visibility maps on real-world terrains. It is also interesting to explore real-world measures used by researchers in fields that predominantly work on terrains scanned from the real world and see if they show a correlation to

the complexity of visibility maps.

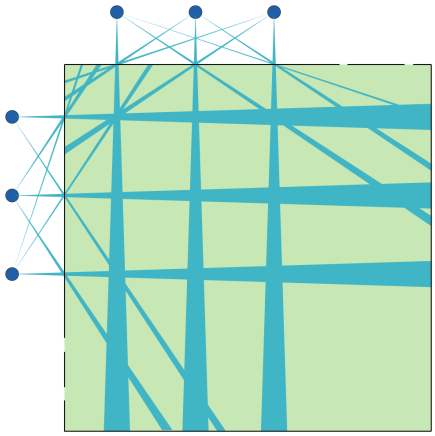

Fig. 2: An example of the *"courtyard"* terrain with $\Omega(m^2n^2)$ complexity, as described by Hurtado *et al.* [1]. The terrain consists of a flat plane surrounded by a thin wall with $O(n)$ windows. Each viewpoint is placed so they all see through each window into the courtyard. The joint viewshed inside the courtyard then forms an $\Theta(mn) \times \Theta(mn)$ grid.

In the field of GIS, a lot of terrain measures are used in the analysis and interpretation of topographic features. These measures are sometimes called topographic attributes (TAs). Dong *et al.* [6] systematically classified a number of these measures based on previous classification methods by scientists in different fields. Most of these measures only provide information for specific parts of a terrain, like catchment areas (basin shaped areas that can collect water) or valleys. Other measures convey information that is unlikely to correlate with viewshed complexity (on their own); examples of this are mean aspect (the direction of a slope) and plane area. From the remaining measures, the ones used for this thesis project were chosen based on their common use being related to visibility or the features they analyze influence viewsheds and thus have the potential to show a correlation with viewshed complexity. The selected measures are *terrain ruggedness index* [7], *terrain shape index* [8], *fractal dimension* [9, 10], *sky visibility index* (a simplification of *solar radiation index* described by Tabik *et al.* [11], and *prickliness*.

Prickliness is a new measure defined by Acharyya *et al.* [12] during the same time as this project, so it is not listed in the paper by Dong *et al.* [6].

Researchers in the different fields that work with terrains use separate ways of representing terrains. GIS and Geology fields primarily use a Digital Elevation Model (DEM), a rectangular 2D raster with elevation values stored in its cells. While computational geometry, graphics, and virtual world fields primarily use a Triangular Irregular Network (TIN), a continuous 3D (Delaunay) triangulation made up of 3D vertices and edges. To create a bridge between these fields (and terrain representations), it is interesting to investigate the behavior of the joint viewsheds and the selected measures on both terrain representations and find out if the same correlations hold between them.

Section 2 contains the definitions of the measures, algorithms, and other concepts used in this project. Section 3 describes the algorithms and adaptions that were implemented specifically for this project. Section 4 contains a description of the experimental setup. The results are listed in Section 5, followed by their interpretation in Section 6. In Section 7, the findings and recommendations based on the results are given. Finally, some recommendations and ideas for possible next steps are discussed in Section 8.

2 Theory and definitions

2.1 Viewsheds

The viewshed of viewpoint p is the set of all visible points on a terrain T. A point q is considered visible if the line $\overline{pq}$ does not intersect T. The joint viewshed is then the union of all viewsheds belonging to the set of all viewpoints P.

To generate the viewsheds for the DEM terrains, we can utilize the *"viewshed 2"* function of the ArcGIS Pro [13] software package. This function uses a brute-force algorithm that tests every cell independently instead of a typical wavefront or sweep line algorithm, which uses an approximate solution (e.g., [14, 15]). *"Viewshed 2"* works by constructing a 3D sightline from each viewpoint to every cell center in the DEM terrain. If a sightline is not obstructed, the target cell is marked as visible.

For this project, the viewshed complexities for the DEM terrains were determined by converting the DEM joint viewsheds to a polygon and counting its vertices. This polygon was constructed using the *"Raster to Polygon"* function of ArcGIS Pro [13] with the *"simplify"* parameter set, so the edges of the polygon become straight line segments instead of conforming to the cell edges.

While ArcGIS Pro [13] provides multiple implementations for viewshed generation on DEM terrains, it does not contain one for TIN terrains. In fact, no publicly available TIN viewshed algorithm could be found. For this reason, the viewsheds for the TIN terrains were generated with an own implementation of the hidden-surface elimination algorithm presented by Goodrich [22]. This algorithm runs in $O(n \log n + k + t)$ time, where n is the number of edges of the terrain, k (resp. t) the number of intersecting pairs of line segments (resp. polygons) created by projecting the edges (resp. triangles) of the terrain onto the 2D projection plane π. This algorithm was chosen for its ease of implementation while still having a good runtime complexity. The details of this implementation are described in Section 3.3.

The viewshed complexities for TIN terrains are the number of vertices on the boundaries of the viewshed arrangement.

2.2 Terrain measures

This section describes the measures used for this project. Most of these measures were only defined for either DEM or TIN terrains. How these were adapted to both formats, while preserving their meaning, is described in Section 3. To explore how the terrain influences viewshed complexity, different strategies are used. Some measures only analyze properties local to a viewpoint, while others consider the terrain as a whole.

2.2.1 Terrain ruggedness index

According to Riley *et al.* [7], the "*Terrain Ruggedness Index* (TRI) provides an objective quantitative measure of topographic heterogeneity." In other words, it shows how variable the elevation of the terrain is. They also state that terrain heterogeneity is an important variable for predicting animal habitats because it helps identify areas that provide cover for prey and stalking cover for predators. Because these traits are tied to visibility, it seems interesting to look at the relation between TRI and joint viewshed complexity.

Calculating TRI is done by summing the squared differences between the elevation of a DEM grid cell and its eight neighboring cells and taking the root of this sum. The measure can be calculated for a whole terrain to identify regions with high change in elevation. TRI is normalized by taking the mean of the sum of squared differences.

$$\begin{aligned} ssdiff &= \frac{1}{N}\sum_{n=0}^{N}((Z_n - Z_v)^2) \\ TRI &= \sqrt{ssdiff} \end{aligned} \tag{1}$$

Where Z_n is the elevation at point n on the circle with radius R, and Z_v is the elevation of the circles' center, which is the viewpoint. For DEM terrains, the points are the cells lying on the circle. Because there is no TRI definition for TIN terrains, this measure was adapted by placing 360 evenly spaced points on the circle for Z_n.

2.2.2 Terrain shape index

The *Terrain Shape Index* (TSI) is a measure described by McNab [8]. It represents the geometric shape of a terrain. In the original paper, it is used for predicting tree height based on landforms.

Mathematically it represents the mean relative difference in elevation between the center of a plot and its circular boundary. The difference in elevation (with respect to the middle point) is sampled N times on the radius R and averaged. For convex topography, the sign of the TSI will be negative because the mean elevation is less than the elevation at the sample point. The sign will be positive for concave topography, and the TSI will be near zero for linear, but not necessarily level, topography. The TSI is normalized by dividing it by R. This makes it equivalent to the mean change in elevation per meter along the radius.

$$\begin{aligned} \bar{Z} &= \frac{1}{N}\sum_{n=0}^{N}(Z_n - Z_v) \\ TSI &= \bar{Z}/R \end{aligned} \tag{2}$$

Where Z_n is the elevation at point n on the circle with radius R, and Z_v is the elevation of the circles' center, which is the viewpoint. For DEM terrains, the points are the cells lying on the radius. Because there is no TSI definition for TIN terrains, this measure was adapted by placing 360 evenly spaced points on the circle for Z_n.

2.2.3 Fractal dimension

First described by Mandlebrot [10], fractal dimension (FD) is an index of terrain complexity that shows how much a pattern changes depending on the scales at which it is measured. Fractal dimension was used by Taud and Parrot [9] to study the relationships between geomorphic features and surface roughness of DEM terrains. They found that using local fractal dimension provides useful information about geological and geomorphic features. They also describe a so-called box-counting method to extract the fractional dimension from a DEM terrain:

A cube of size $s \times s \times s$ is centered on a point that lies on the terrain's surface. The volume under the surface is filled up by a set of voxels, the sides of which are equal to the DEM cell size. The cube contains a tower of 0 to s voxels, based on the terrain's elevation, at each (x, y) coordinate within it. The cube is then partitioned in boxes of size q varying between 1 and $s/2$, depending on the whole dividers of s. Each of these boxes is considered as filled if at least one voxel is contained in this box. The variable box size q and the resulting amount of filled boxes n are recorded, and their log values are graphed. The fractal dimension is then the inverse of the slope of the linear regression line. Figure 3 shows an example of the box-counting method, with the accompanying graph in Figure 4.

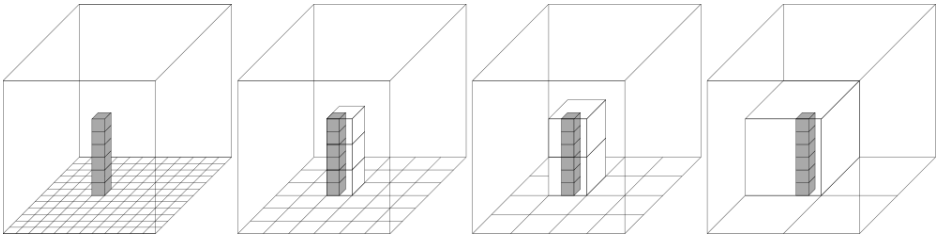

Fig. 3: Local fractal dimension with $s = 12$, $q = 1, 2, 3, 6$, and $N = 6, 3, 2, 1$.

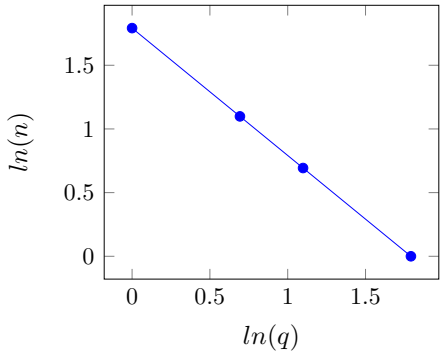

Fig. 4: Graph of the box-counting example in Figure 3, the slope of the line is -1, taking the inverse results in a fractal dimension of 1.

2.2.4 Sky visibility index

Initially, *"solar radiation index"* [11] was selected as one of the experimental measures because it calculates the amount of solar radiation parts of the terrain receive. This solar radiation can be limited by the obstructions between the measured point on the terrain and the sun. This description is similar to a visibility problem because the "visibility" of the sun at a point on the terrain is tested. Upon further inspection, however, this measure also considers data that is not relevant to viewsheds. Examples of this are the time, day, year, light transmittivity through the sky, and the path the sun travels over the terrain. To extract only the visibility component and reduce its computational complexity, *"solar radiation index"* was simplified to a *"sky visibility index."*

In this project, *"Sky visibility index"* is defined as the visible percentage of a horizontal skydome centered on a viewpoint (see Figure 5 for a 2D example). ArcGIS Pro [13] has a *"skyline"* tool built-in, which generates the skylines for multiple viewpoints and a DEM or TIN terrain. The *"skyline graph"* tool returns the percentage of visible sky based on these skylines. Because at higher points of the terrain there are fewer obstructions, this measure should, in theory, be higher at peaks and lower in pits. Kim *et al.* [16] showed a similar trend regarding viewshed coverage: By placing viewpoints at peaks, viewshed coverage increases, and by placing viewpoints in pits, viewshed coverage decreases as well.

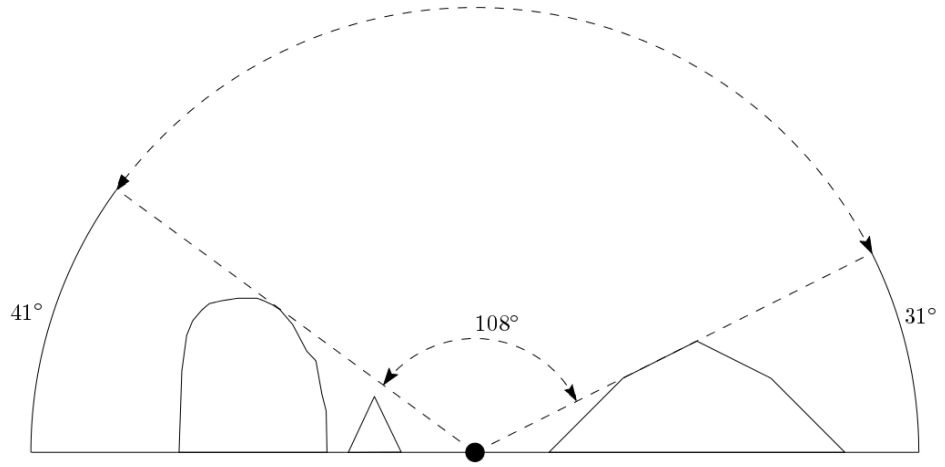

Fig. 5: An example of sky visibility in 2D. A horizontal dome centered on the viewpoint is placed around the terrain. A skyline is drawn based on the obstructing terrain, then the percentage of visible sky is calculated based on this skyline. In this example, the left mountain obstructs 41°, and the right mountain 31°. The total dome is 180°, so the *sky visibility index* is $\frac{108}{180} = 0.6$.

2.2.5 Prickliness

Prickliness is a terrain-wide measure defined by Acharyya *et al.* [12] specifically to show the potential of 2.5D terrains to have high complexity viewsheds. It is defined as such:

The formal definition by Acharyya *et al.* [12] is as follows; Let T be an xy-monotone terrain. Let A be an affine transformation. The local maxima of $A(T)$, $m(A(T))$, is the number of internal and convex vertices of T which are extremal in the z-direction. That is, all adjacent vertices have a lower or equal z-coordinate. Let $\mathcal{A}(T)$ be the set of all affine transformations of T. The *prickliness* of T, $\pi(T)$ is then defined as the maximum number of local maxima over all transformations of T.

In simpler terms, let $\vec{v}$ be a vector in $\mathbb{R}^3$, let $\pi_{\vec{v}}(T)$ be the number of local maxima of terrain T in direction $\vec{v}$. That is, the points in T that do not allow further traversal in direction $\vec{v}$. (For a vector along the z-axis, this would be the points on the terrain where the surrounding points are all at a

lower elevation.) The prickliness $\pi(T)$ for T is then the maximum number of local maxima over all directions.

Observe that to traverse from vertex v to an adjacent vertex v_a in direction $\vec{v}_t$, the dot product of the vectors (v, v_a) and $\vec{v}_t$ has to be positive. The directions for which this is true and false can be separated by a plane perpendicular to (v, v_a) and passing through v. Then the cone constructed by all the perpendicular planes belonging to v and its adjacent vertices contains all the directions for which v is a local maximum.

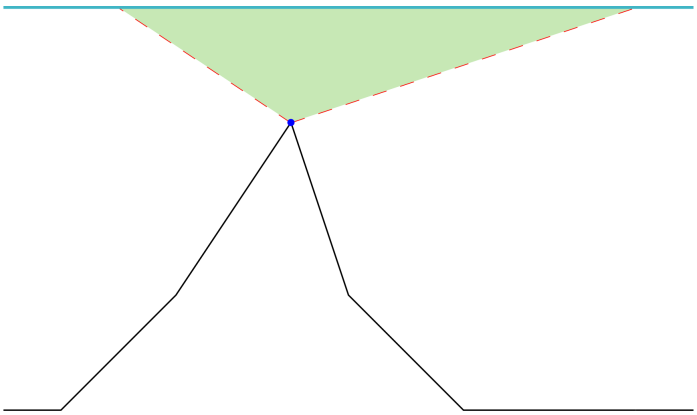

Fig. 6: A 2D representation of the prickliness cone. Planes (red dashed lines) are placed perpendicular to the edges adjacent to vertex v, passing through v. For all the directions originating from v and pointing "above" all the perpendicular planes, v is a local maximum. This region (green) is recorded on a horizontal plane (light blue line), with its origin translated slightly above v. The region on the 2D plane with the most overlapping viewshed cone fragments contains the prickliness direction(s). The number of overlapping cones within this region is the prickliness $\pi(T)$ for terrain T.

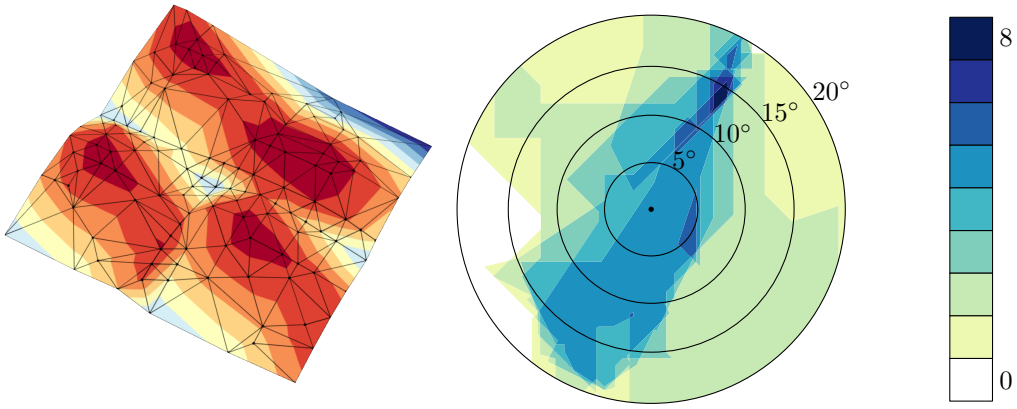

Fig. 7: An example of a TIN terrain (left) and the accompanying 2D arrangement of local maxima (right). The colors in the arrangement indicate the number of local maxima in direction $\vec{v}$ in degrees from direction vector (0,0,1). The *prickliness* is 8 in the directions roughly 13° north-east from the origin.

3 Implemented algorithms and datasets

Several algorithms had to be implemented, and a dataset was created to run the experiments for this project. The algorithms were implemented because they were conceived explicitly for this project, or there was no publicly available implementation. If (legally) possible, the implementations of these algorithms and datasets will be made publicly available for future research.

3.1 Terrain datasets

To make the results statistically significant, a dataset of 52 terrains with equal dimensions but different elevation properties was created by identifying, extracting, and processing regions of the real world with varying terrain configurations. The gathering of these terrains was done using the "terrain" world elevation layer [19] provided by the Environmental Systems Research Institute (ESRI) using the ArcGIS Pro software package [13]. The terrain extents of these terrains are listed in appendix A.

Each of the gathered terrains has a cell size of 10 meters and a dimension of 1400 rows by 1200 columns, the total size being $14000m \times 12000m$. Zhang *et al.* [20] found a DEM resolution of 10 meters to be the best compromise between high resolution and processing time of measurements. More recently, Maynard *et al.* [21] found that moderate resolutions (i.e., 10 to 20 meters) accurately represent terrain features while fine resolutions (i.e., 1 to 5 meters) only provide a marginal improvement in accuracy of various terrain measures while increasing computational requirements. Finally, because a resolution of 10 meters seems to be used often within the GIS field, and thus widely available, it is the obvious choice.

The TIN terrains were also generated with the ArcGIS Pro software package [13] using the *"Raster to TIN"* function. This function generates a Delaunay triangulation to avoid long, thin triangles as much as possible.

3.2 Adaption of measures

Most of the measures used in this project were described only for either DEM terrains or TIN terrains. To be able to run all experiments on both terrain representations, their counterparts had to be conceived and implemented.

3.2.1 TRI and TSI

TRI and TSI are defined explicitly for DEM terrains. Both of these measures use the elevation difference between the viewpoint and the elevation of the DEM cells lying on a circle centered on that viewpoint. All the DEM cells that intersect a circle with a given radius are measured (Figure 8.) In essence, these measures use an approximation of the elevation values under a circle. Because there is no definition for TIN terrains, these measures were adapted by measuring the elevation at 360 evenly spaced points on the circle centered on the viewpoint.

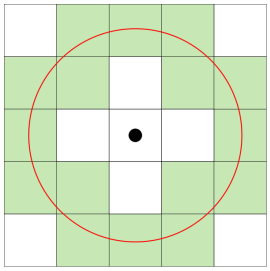

Fig. 8: To adapt the *TRI* and *TSI* measures for larger radii, the elevation values of the (green) cells lying underneath the (red) circle were counted for these measures.

3.2.2 Fractal Dimension

For this project, fractal dimension was adapted for TIN terrains while adhering to the same method described in Section 2.2.3. To obtain the voxel surface at a viewpoint, equal distant points in the xy plane were taken, originating from the viewpoint. The distance between the points was determined by the voxel size v, and the number of stacked voxels at each point was determined with $\lceil \frac{z_{xy}}{v} \rceil$, where z_{xy} is the elevation at the (x, y) coordinate.

3.2.3 Prickliness

Using the observation from Section 2.2.5, an $O(n^2)$ algorithm for TIN terrains was developed (with Acharyya *et al.* [12]) and implemented using CGAL [17] and its *"2D arrangements"* [18] library. It works in the following steps:

1. For each interior vertex v of T, iterate through every adjacent vertex v_a of v. Construct a plane perpendicular to the vector (v, v_a) passing through v. Intersect this plane with a horizontal plane with its origin placed slightly above v. The intersecting line marks a boundary of the region of local maxima vectors for v.

2. These lines are added to a 2D arrangement M creating regions where the numbers of local maxima are equal.

3. After iterating through all vertices, perform a breadth-first traversal of M starting by determining the number of local maxima m in an arbitrary face and traversing over the boundaries. When traversing

over a boundary increment (resp. decrement) m for every local maxima cone we enter (resp. exit). Note that being inside a cone means being above all the perpendicular planes belonging to it.

4. Finally, return the highest number of local maxima within the arrangement as the *prickliness*.

The *prickliness* values for the DEM terrains were approximated because the DEM terrains have significantly more vertices (cell centers) and a constant eight neighbors, this causes a significant increase in computation time and, more importantly, memory usage. The approximation algorithm translates a horizontal grid G of n by n and cell size s above the cell center c_t of each interior cell. The vectors originating from c_t to every cell center in G are then tested and counted for being a local maximum (i.e., if it is contained within the local maxima cone). Cell size s was set to 0.05, based on the results of the TIN terrains. This method should, in practice, produce a close approximation of prickliness.

3.3 Goodrich viewshed algorithm

While ArcGIS Pro [13] provides multiple implementations for viewshed generation on DEM terrains, it does not contain one for TIN terrains. In fact, no publicly available TIN viewshed algorithm could be found. The hidden-surface elimination algorithm presented by Goodrich [22] was selected to generate the viewsheds for the TIN terrains. This algorithm runs in $O(n \log n + k + t)$ time, where n is the number of edges of the terrain, k (resp. t) the number of intersecting pairs of line segments (resp. polygons) created by projecting the edges (resp. triangles) of the terrain onto the 2D projection plane π. This algorithm was chosen for its ease of implementation while still having a good runtime complexity. It works in four steps:

1. Project the set of 3D polygons P onto a 2D plane π and store this in a 2D arrangement based on a doubly connected edge list (DCEL).

2. Construct *"overlap relation"* R, a directed graph with every node corresponding to a polygon and each edge storing the spatial order and overlap relations between the polygons.

3. Using R, sort the polygons back-to-front.

4. Using the *"painter's algorithm"* "draw" the 2D polygons back to front, removing previously visible edges within the newly added 2D polygon.

The final arrangement contains the 2D projection of the 3D viewshed, with every half-edge containing a 3D polygon index. To project these half-edges back into 3D, a ray is shot through both edge points. An intersection test is then performed on the 3D polygon creating a 3D edge from the intersection points. Combining these 3D edges forms the viewshed.

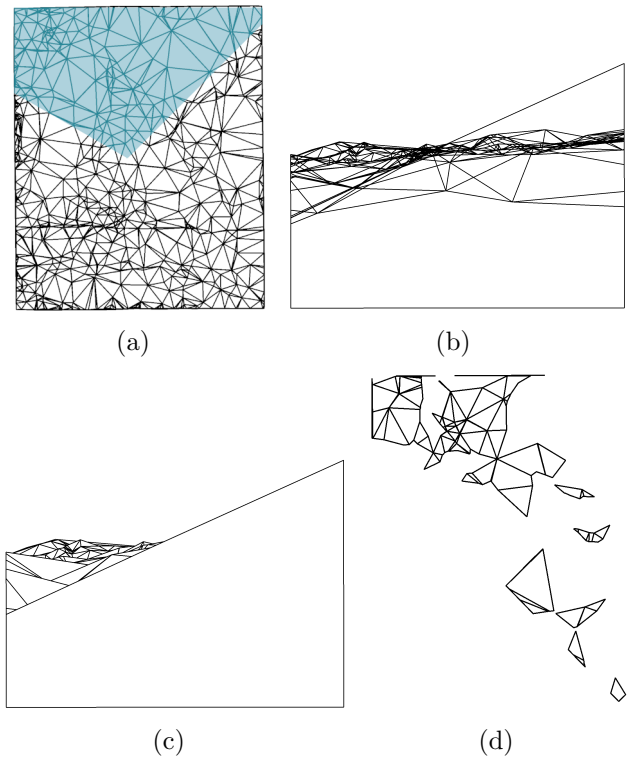

Fig. 9: An example of viewshed generation using the implemented Goodrich hidden-surface elimination algorithm [22]. Figure (a) shows a terrain with a view frustum in blue, originating from a viewpoint in the center. Figure (b) shows the 2D projection of the polygons inside the view frustum. Using the overlap relation graph and painter's algorithm, the obscured (parts of) polygons are removed, resulting in Figure (c). Finally, the polygons are projected back into 3D, producing the final viewshed in Figure (d).

The *"painter's algorithm"* works by drawing the 2D polygons one-by-one starting with the furthest polygon. When a newly added polygon P_n overlaps the previously added polygon(s), the edges inside P_n are removed using a depth-first search on the inner edges connected to the boundary vertices of P_n. Note that this operation can create redundant vertices on the edges of P_n. These have to be removed as not to inflate the viewshed complexity.

The overlap relation graph R is constructed by traversing the boundary of each polygon projected onto π. When the boundaries of two polygons intersect, their obscure/obscures relation is stored in R depending on their spatial ordering. Polygons are fully embedded if its boundary edges do not intersect the boundary of another polygon. When a fully embedded polygon is stored in R and obscures another polygon, it can simply be "drawn," and the depth-first search can be skipped. Polygons that are fully embedded and are obscured by another polygon are always invisible, so they are simply removed.

The viewsheds from multiple viewpoints were overlaid using the algorithm described by Finke and Hinrichs [23], as suggested by Hurtado *et al.* [1]. Because the algorithm by Goodrich [22] is described for a view frustum, it was adapted to all directions by projecting the terrain onto a unit cube centered on the viewpoint and processing each side individually before stitching the results together.

4 Experimental setup

Two software pipelines were set up to facilitate the automated testing of a potentially large amount of terrains, one for the DEM terrains and another for the TIN terrains. The pipeline for DEM terrains was developed with python using the ArcPy library included with ArcGIS Pro [13]. This library does not contain arbitrary-precision floating-point operations, but it is a widely used software package within the geosciences and contains many tools for DEM terrains.

The pipeline for TIN terrains was implemented using C++ and the CGAL library [17], which does support arbitrary floating-point operations. CGAL is well-known within the computational geometry field and provides multiple algorithms and data structures that facilitate working with continuous surfaces like TIN terrains. CGALs *"2D arrangements"* [18] library was used to compute the viewsheds and prickliness.

The experiments are run for each terrain in the following manner:

1. Pre-process the terrain
2. Generate viewpoint sets
3. Generate viewsheds
4. Run measures
5. Export results

The pre-processing step mostly applies to the DEM terrains. It generates the TIN version (if it does not exist) and adds the spatial reference *"WGS 1984 Web Mercator (auxiliary sphere)"* needed by ArcGIS Pro to run some of the measures. The exported results are used in the statistical analysis.

4.1 Viewpoints

The viewpoints were generated within an evenly spaced grid to prevent clustering, with one viewpoint per cell. Kim *et al.* [16] found that placing the viewpoints at peaks produces viewsheds that cover hilltops, but not many valleys. Placing them in pits produces the opposite, and passes a combination of the two. Three sets of viewpoints were generated for every terrain to cover these different cases, with each viewpoint located on the highest, lowest, and random point within their respective grid cell.

When viewpoints are placed close to the boundary of a terrain, measures that use a radius or window size could extend past the terrains' boundary. A margin around the grid was added with its width set to the radius/window half-size used in the measures to prevent this. Because a typical observer (e.g., a person) is at least a meter above the ground, the viewpoints were offset to 1 meter above the surface. This offset also prevents artifacts caused by viewpoints being underneath the terrain due to rounding errors. Both viewpoint sets use the same xy-coordinates to make the DEM and TIN datasets more comparable. Because elevation values are not equal between the two terrain types, the z values of the viewpoint are re-interpolated for both datasets. The number of viewpoints was set to 9 in a 3×3 grid. This amount typically does not cover the whole terrain and provides a good spread.

Another dataset with a single viewpoint was also generated to explore the change in behavior between single and multiple viewpoints. This dataset was generated in the same way as the multiple viewpoint dataset to make the results comparable. The single viewpoint was generated in the middle cell of a 3×3 grid.

4.2 Terrains

For this project, a dataset of 52 DEM terrains was created using the "terrain" world elevation layer [19] provided by the Environmental Systems Research Institute (ESRI) using the ArcGIS Pro software package [13]. The terrain extents of these terrains are listed in appendix A. Each of the gathered terrains has a cell size of 10 meters and a dimension of 1400 rows by 1200 columns, the total size being $14000m \times 12000m$. Zhang *et al.* [20] found a DEM resolution of 10 meters to be the best compromise between high resolution and

processing time of measurements. More recently, Maynard *et al.* [21] found that moderate resolutions (i.e., 10 to 20 meters) accurately represent terrain features while fine resolutions (i.e., 1 to 5 meters) only provide a marginal improvement in accuracy of various terrain measures while increasing computational requirements. Finally, because a resolution of 10 meters seems to be used often within the GIS field, and thus widely available, it is the obvious choice.

The TIN terrains were also generated with the ArcGIS Pro software package [13] using the *"Raster to TIN"* function. This function generates a Delaunay triangulation to avoid long, thin triangles as much as possible. With the *z-tolerance* setting, the triangulation complexity can be controlled by determining an allowed deviation from the DEM elevation values. Initially, a z-tolerance of 100 meters was used. This z-tolerance generated TIN terrains that ensured reasonable processing times. To further explore certain measures' behavior and come closer to the detail level of the DEM terrains, a TIN terrain set with a z-tolerance of 50 meters was also generated.

4.3 Statistical analysis

After running the experiments, each measure and viewshed complexity combination is loaded into a scatterplot to determine the relationship's shape and identify patterns. Linear regression was performed on these combinations using Pearson's r, using the following value thresholds:

Strong linear correlation	$0.9 < r \leq 1.0$
Medium linear correlation	$0.7 < r \leq 0.9$
Weak linear correlation	$0.5 < r \leq 0.7$
No or doubtful linear correlation	$0.0 < r \leq 0.5$

For interesting correlation values, the significance was determined by looking at the R^2 values and scatter plots. The R^2 values were roughly interpreted in the following manner:

Strong effect size	$0.7 < R^2 \leq 1.0$
Moderate effect size	$0.5 < R^2 \leq 0.7$
Weak or low effect size	$0.3 < R^2 \leq 0.5$
None or very weak effect size	$0.0 < R^2 \leq 0.3$

5 Results

After running the experiments, the values obtained from the measures were tested for correlation with the accompanying viewshed complexities. This section starts with the results for a single viewpoint on the terrains, then multiple viewpoints, and finally, the higher complexity TINs. To keep this section clearer, it contains the scatter plots for the prickliness with the highest viewpoints because they are the most interesting. The other plots can be found in appendix B.

5.1 Single viewpoints

Table 1 shows the linear regression results between the measures and the *viewshed complexity* of a single viewpoint on the DEM terrains. All the measures show no to weak correlation values. The correlation between *prickliness* and the *viewshed complexity* is the highest with a positive correlation value of 0.629. The accompanying graph (Figure 10) and the R^2 value shows this not to be very significant.

	Single viewpoint on DEM terrains					
	Highest		Lowest		Random	
Measures	R	R^2	R	R^2	R	R^2
Sky visibility index	0.114	0.013	0.321	0.103	0.345	0.119
Prickliness	0.629	0.396	0.100	0.010	0.176	0.031
Terrain ruggedness index	-0.402	0.162	-0.278	0.078	-0.261	0.068
Terrain shape index	-0.399	0.159	-0.278	0.077	-0.261	0.068
Fractal Dimension	0.272	0.074	0.220	0.048	0.275	0.076

Tab. 1: The correlation R and accompanying R^2 values between the terrain measures and the DEM terrains' viewshed complexities with a single viewpoint.

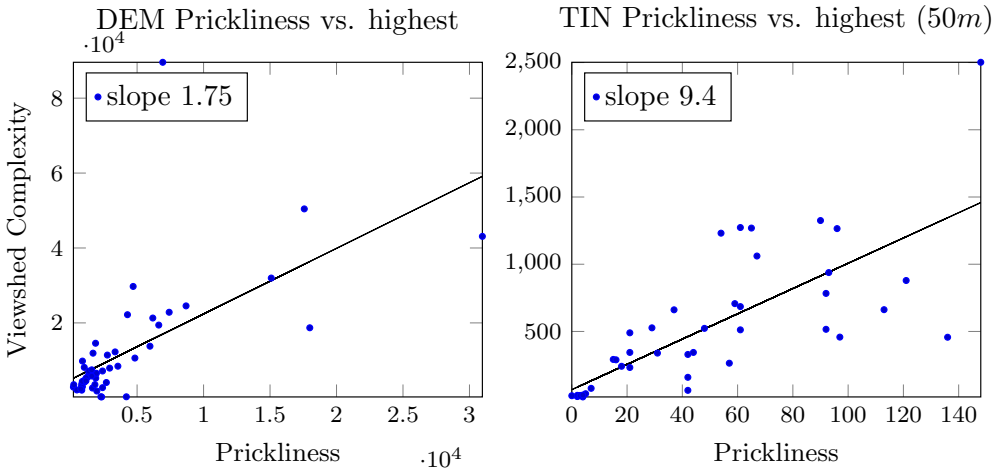

Fig. 10: The scatter plots for the DEM (left) and TIN (right) prickliness and viewsheds originating from a single viewpoint placed at the highest point.

The results for the viewshed complexity from a single viewpoint on the TIN terrains (Table 2) show a better correlation for the TRI and TSI values. These correlation values are also consistent across the three viewpoint selection procedures, with a weak positive correlation of around 0.500. However, the scatter plots for these two measures show a large variation, and the R^2 values show these not to be significant. Prickliness shows an improvement on TIN terrains with a weak to moderate correlation, especially when placing the viewpoints at the highest points. However, the lowest and random points still show a large variance.

	Single viewpoint on TIN terrains					
	Highest		Lowest		Random	
Measures	R	R^2	R	R^2	R	R^2
Sky visibility index	-0.041	0.002	-0.451	0.204	-0.610	0.372
Prickliness	0.746	0.556	0.414	0.172	0.637	0.405
Terrain ruggedness index	0.552	0.305	0.498	0.248	0.595	0.354
Terrain shape index	0.552	0.304	0.403	0.162	0.430	0.185
Fractal Dimension	-0.047	0.002	-0.096	0.009	-0.499	0.249

Tab. 2: The correlation R and accompanying R^2 values between the terrain measures and the viewshed complexities of the TIN terrains with a single viewpoint.

5.2 Multiple viewpoints

For the viewsheds of the DEM terrains originating from 9 viewpoints, none of the measures seem to have a statistical significance, with most of the R^2 values being below 0.200. The exception to this is the correlation between *prickliness* and the joint viewsheds originating from the viewpoints placed on the highest points. With a correlation of 0.9 and an R^2 value of 0.810, this measure shows a very strong relationship and high significance.

	Multiple viewpoints on DEM terrains					
	Highest		Lowest		Random	
Measures	R	R^2	R	R^2	R	R^2
Sky visibility index	0.205	0.042	0.394	0.155	0.458	0.210
Prickliness	0.900	0.810	0.194	0.038	0.644	0.415
Terrain ruggedness index	-0.374	0.140	-0.332	0.110	-0.419	0.175
Terrain shape index	-0.373	0.139	-0.346	0.120	-0.415	0.172
Fractal Dimension	0.357	0.127	0.471	0.222	0.318	0.101

Tab. 3: The correlation R and accompanying R^2 values between the terrain measures and the viewshed complexities of the DEM terrains with nine viewpoints.

The correlation values on the $100m$ z-tolerance TIN terrains are all higher than on the DEM terrains. *Sky visibility*, *terrain ruggedness index*, and *terrain shape index* all show a moderate (negative) correlation with a weak to moderate significance. *Prickliness* shows very strong correlation values with high significance on all viewpoint variations. The scatter plots for these measures show the same. *Sky visibility*, *terrain ruggedness index*, and *terrain shape index* show a slight to moderate variance from the regression line. *Prickliness* shows a very clear linear relationship (see Figure 11).

	Multiple viewpoints on TIN terrains (100m)					
	Highest		Lowest		Random	
Measures	R	R^2	R	R^2	R	R^2
Sky visibility index	-0.716	0.513	-0.847	0.718	-0.884	0.782
Prickliness	0.952	0.907	0.896	0.804	0.949	0.901
Terrain ruggedness index	0.735	0.540	0.829	0.688	0.837	0.700
Terrain shape index	0.728	0.530	0.806	0.650	0.830	0.690
Fractal Dimension	-0.715	0.511	-0.374	0.140	-0.698	0.487

Tab. 4: The correlation R and accompanying R^2 values between the terrain measures and the viewshed complexities of the TIN terrains with nine viewpoints. The TIN terrains for these results were generated with a z-tolerance of 100 meters.

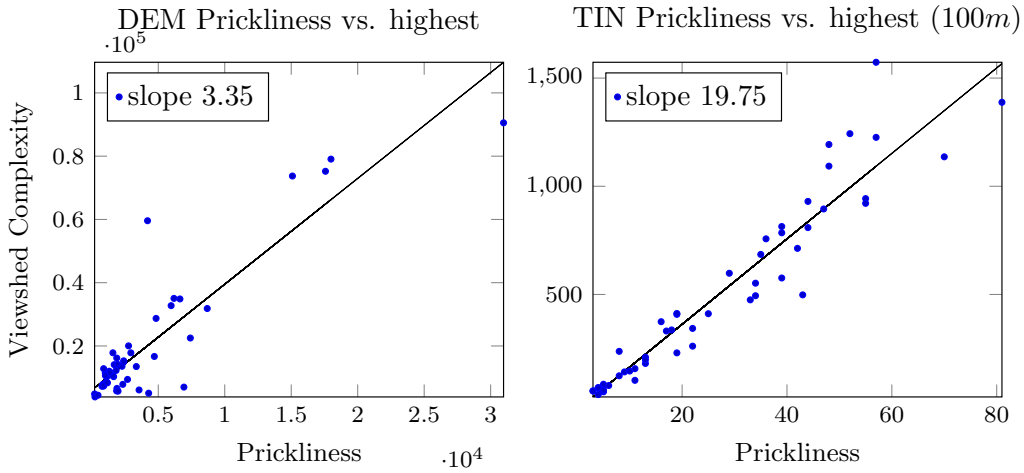

Fig. 11: The scatter plots for the DEM (left) and 100m TIN (right) prickliness and viewsheds originating from a single viewpoint placed at the highest point.

5.3 Higher complexity TINs

To explore the difference in correlation between DEM and TIN terrains, TIN terrains were re-generated with a lower z-tolerance, and the experiments were re-run on these. The lower z-tolerance increases the complexity of the TIN terrains and brings them closer to the DEM terrains' detail level. The results of this experiment show a slight drop in correlation for all measures except *prickliness*, and the accompanying scatter plot for prickliness shows a wider variance (Figure 12). These results indicate that the measures are sensitive to higher complexity terrains, and more information is needed to improve the correlation with the complexity of the joint viewsheds.

	Multiple viewpoints on TIN terrains (50m)					
	Highest		Lowest		Random	
Measures	R	R^2	R	R^2	R	R^2
Sky visibility index	-0.644	0.415	-0.739	0.546	-0.770	0.592
Prickliness	0.968	0.937	0.832	0.692	0.932	0.869
Terrain ruggedness index	0.674	0.455	0.731	0.534	0.710	0.504
Terrain shape index	0.699	0.488	0.679	0.461	0.668	0.446
Fractal Dimension	-0.555	0.308	-0.345	0.119	-0.753	0.566

Tab. 5: The correlation R and accompanying R^2 values between the terrain measures and the viewshed complexities of the TIN terrains with nine viewpoints. The TIN terrains for these results were generated with a z-tolerance of 50 meters.

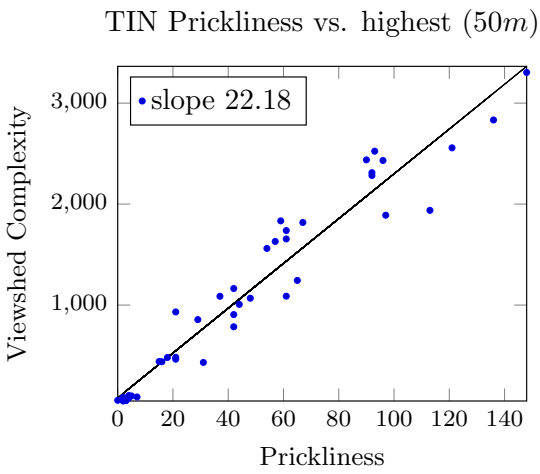

Fig. 12: The scatter plot for the 50m TIN prickliness and viewsheds originating from a single viewpoint placed at the highest point.

6 Discussion

The *terrain ruggedness index (TRI)* and *terrain shape index (TSI)* measures do not seem to be a good predictor of viewshed complexity on high complexity terrains. This could be explained by the fact that TRI and TSI measure at set radii from the viewpoints, which can result in a lack of information because sight obstructions can be placed at any distance from the viewpoint. When looking at the results, both of these measures show a moderate correlation with joint viewshed complexity on the lowest complexity terrains (Table 4). However, when the terrains become more detailed, they show a clear drop in correlation (Table 5). This drop is further supported by the results on the DEM terrains (Table 3), which at a resolution of 10 meters, preserves the smaller obstructions to a higher degree than the TIN terrains. Finally, these measures show even worse correlation when only using a single viewpoint (Tables 1 & 2), which decreases the amount of information gathered on the terrain compared to the nine viewpoints that have been spread over the terrain.

The results for the *fractal dimension* measure are harder to explain. Unlike the *TRI* and *TSI*, it considers the variability within an area of the terrain as opposed to a radius. Taking a closer look at the fractal dimension values for both terrain datasets shows a minimal variation, with most of them being close to 3.0, which, according to Taud *et al.* [9], indicated a near-constant terrain. These results seem to indicate that this measure fails to detect the variation in elevation levels with the chosen parameters.

The *sky visibility index* inversely links to viewshed complexity to a limited extent. A trivial example of this is a flat terrain; the sky is completely visible while viewshed complexity is low. When adding obstructions, inevitably, parts of the sky become covered, which reduces the sky visibility index. While this measure is not affected by range, the limiting prediction factor could be explained by the observation that, in a particular direction, only the obstruction with the largest angle with respect to the viewpoint gets counted. This results in lower obstructions not being counted in this measure but still contributing to viewshed complexity. As the results show, this causes the sky visibility index to correlate less when the terrain's complexity increases.

For TIN terrains, the results show that *prickliness* correlates very well with viewshed complexity, especially when the viewpoints are placed on the highest points. For DEM terrains, this seems *only* to be the case for viewsheds originating from the highest points. When the viewpoints are placed at the lowest points of the DEM terrains, the correlation disappears. Prickliness measures the peaks in the terrain in all directions in the positive z-axis. This means that when a viewpoint is placed at the highest elevation and the viewshed gets split up by the protrusions (which seem to be accurately tracked by prickliness), there is a strong correlation. However, when the viewpoints are placed at the lowest points, the viewsheds become severely limited by the walls of the pits or valleys in which they are placed. Even when placing multiple viewpoints, these viewsheds do not seem to encounter enough of the protrusions that are detected by the prickliness measure. The difference between the results on the TIN and DEM terrains for prickliness can once again be attributed to the higher detail level the DEM dataset offers; the TIN terrains contain few small pits resulting in viewsheds that still cover large parts of the terrain and thus encounter more of the complexity increasing protrusions.

The main reason why prickliness performs so well compared to the other measures is also mentioned by Acharyya *et al.* [12]. While obstructions are, of course, a difference in elevation, the height of the obstruction does not necessarily matter. For example, if there is a column in front of the viewpoint, the viewshed will be split regardless of its height. Thus measuring only the elevation difference could paint the wrong picture of what is actually affecting the viewshed's complexity. This gives prickliness an advantage because it detects the protrusions of the whole terrain without considering their elevation.

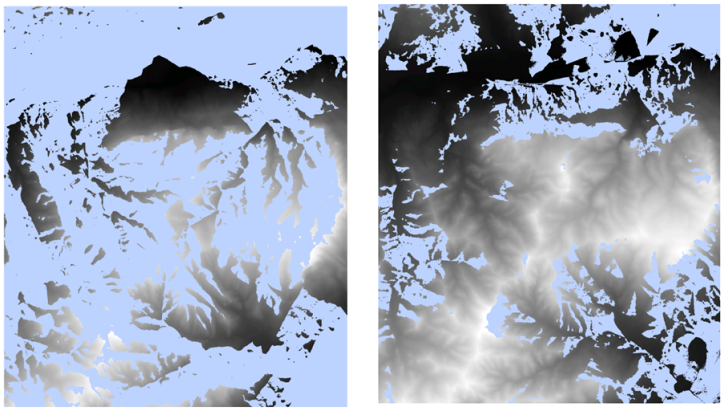

(a) (b)

Fig. 13: Left a joint viewshed (blue) created from viewpoints placed on the highest points. Right a joint viewshed (blue) created from viewpoints placed on the lowest points.

7 Conclusion

This thesis project took multiple measures from different GIS fields and explored their correlation with (multiple) viewshed complexity on real-world terrains. The behaviors of the selected measures and viewsheds were explored on both TIN and DEM terrain representations to create a bridge between the different scientific fields using them. The results of the project differ greatly between these two terrain representations. TIN terrains show a moderate to strong correlation with most of the measures, but the DEM terrains show mostly the opposite. A more detailed discussion on the findings for the individual measures has been provided in Section 6.

The divide in the ability to predict viewshed complexity can be largely attributed to the difference in resolution. DEM terrains offer a very fine resolution while maintaining a predictable and easily exploitable grid format. 10 meters was used in this case, but even a DEM resolution of 1 meter or less is available for some parts of the world. On the other hand, TIN terrains are harder to work with. Computing the viewsheds and measures on TIN terrains is computationally (and algorithmically) more complex and put a limitation on the resolution used in this project. When generating TIN terrains from DEM terrains, z-tolerances below 50 meters increase the

number of vertices, and thus space/time complexity, dramatically. However, to preserve the small protrusions on the terrain, which significantly affect the viewshed complexity, a small z-tolerance is required.

When working with TIN terrains of similar complexity, *sky visibility index*, *terrain ruggedness index*, and *terrain shape index* can be used to get a quick (but rough) idea of the viewshed complexity. However, the correlation values of these measures deteriorate when increasing the resolution of the terrain.

For TIN terrains, *prickliness* has a very strong correlation with the viewshed complexity of multiple viewpoints. On DEM terrains, only prickliness, in combination with viewsheds origination from multiple viewpoints placed on the highest points of the terrain, shows a strong correlation. In comparison, the other measures show no statistically significant correlation. Placing the viewpoints on the peaks of the terrain is a common procedure if, for example, the goal is to maximize the viewshed coverage (e.g., guard placement, radio towers) [16, 2]. Based on our results, it is recommended to use prickliness as a measure to predict the complexity of the viewsheds in these use cases.

8 Future work

There are many possible experiments that could provide more insight into viewshed complexity, especially when the viewpoints are placed on lower elevations. One key observation seems to be that elevation difference is a good indicator of viewshed coverage [16], but this does not seem to be the case for viewshed complexity. Therefore, it is interesting to also look at measures that detect terrain variability without (only) looking at elevation (e.g., [24]). There also seems to be a difference in predicting viewshed complexity for single viewpoints versus multiple viewpoints. Measures that consider the whole terrain could negatively affect the correlation with single viewpoint viewshed complexity because these viewsheds are usually limited to a subset of the terrain. Combining several measures to take into account the effects of peaks *and* pits should also improve the correlation values.

While *prickliness* maintains a very strong correlation when the viewpoints are placed on the peaks of the terrain, placing them in the pits of the terrain

negatively affects the correlation. With these observations in mind, attempts could be made to improve this measure. One simple idea might be to look at a "negative" prickliness that looks at local minima instead of local maxima.

For the simpler measures like *terrain ruggedness index* and *terrain shape index*, which use a local window/radius, multiple sizes could be combined to (for example) detect near, mid, and far terrain variability.

Finally, more insight could also be gained from experiments on the effects of DEM and TIN resolutions. The results of this project show considerable variability between the different resolutions that were used.

References

[1] F. Hurtado, M. Löffler, I. Matos, V. Sacristán, M. Saumell, R. I. Silveira, and F. Staals, "Terrain visibility with multiple viewpoints," *Lecture Notes in Computer Science (including subseries Lecture Notes in Artificial Intelligence and Lecture Notes in Bioinformatics)*, vol. 8283 LNCS, pp. 317–327, 2013.

[2] F. Kammer, M. Löffler, P. Mutser, and F. Staals, "Practical Approaches to Partially Guarding a Polyhedral Terrain," in *Lecture Notes in Computer Science*, 2014, vol. 8728, pp. 318–332. [Online]. Available: http://link.springer.com/10.1007/978-3-319-11593-1{_}21

[3] L. De Floriani, P. Marzano, and E. Puppo, "Line-of-sight communication on terrain models," *International Journal of Geographical Information Systems*, vol. 8, no. 4, pp. 329–342, 1994.

[4] I. R. Lake, A. A. Lovett, I. J. Bateman, and I. H. Langford, "Modelling environmental influences on property prices in an urban environment," *Computers, Environment and Urban Systems*, vol. 22, no. 2, pp. 121–136, 1998.

[5] M. W. Lake, P. E. Woodman, and S. J. Mithen, "Tailoring GIS software for archaeological applications: An example concerning viewshed analysis," *Journal of Archaeological Science*, vol. 25, no. 1, pp. 27–38, 1998.

[6] Y. Dong, G. Tang, and T. Zhang, "a Systematic Classification Research of Topographic Descriptive Attribute in Digital Terrain Analysis," *The International Archives of the Photogrammetry, Remote Sensing and Spatial Information Sciences*, vol. 37 B2, pp. 357–362, 2008.

[7] S. Riley, S. DeGloria, and R. Elliot, "Index That Quantifies Topographic Heterogeneity," *Intermountain Journal of Sciences*, vol. 5, pp. 23–27, 1999.

[8] W. Henry McNab, "Terrain shape index: Quantifying effect of minor landforms on tree height," *Forest Science*, vol. 35, pp. 91–104, 03 1989.

[9] H. Taud and J.-F. Parrot, "Measurement of DEM roughness using the local fractal dimension," *Géomorphologie : relief, processus, environnement*, vol. 11, no. 4, pp. 327–338, 2005.

[10] B. B. Mandelbrot, *The fractal geometry of nature.* New York: W.H. Freeman, 1982.

[11] S. Tabik, A. Villegas, E. L. Zapata, and L. F. Romero, "A fast GIS-tool to compute the maximum solar energy on very large terrains," in *Procedia Computer Science*, vol. 9, 2012, pp. 364–372.

[12] A. Acharyya, R. K. Jallu, M. Löffler, G. G. T. Meijer, M. Saumell, R. I. Silveira, and H. R. Tiwary, "Terrain prickliness: theoretical grounds for high complexity viewsheds," pp. 1–3, 2020.

[13] Environmental Systems Research Institute (ESRI), "Arcgis pro (2.5.1)," 05 2020. [Online]. Available: http://pro.arcgis.com/

[14] W. R. Franklin and C. K. Ray, "Higher isn't necessarily better: visibility algorithms and experiments," *Advances in GIS research. Proc. 6th symposium, Edinburgh, 1994. Vol. 2*, pp. 751–770, 1994.

[15] M. Kreveld, "Variations on Sweep Algorithms: efficient computation of extended viewsheds and class intervals," *In Proc. 7th Int. Symp. on Spatial Data Handling*, pp. 1–14, 1996.

[16] Y. H. Kim, S. Rana, and S. Wise, "Exploring multiple viewshed analysis using terrain features and optimisation techniques," *Computers and Geosciences*, vol. 30, no. 9-10, pp. 1019–1032, 2004.

[17] The CGAL Project, *CGAL User and Reference Manual*, 5th ed. CGAL Editorial Board, 2020. [Online]. Available: https://doc.cgal.org/5.0.2/Manual/packages.html

[18] R. Wein, E. Berberich, E. Fogel, D. Halperin, M. Hemmer, O. Salzman, and B. Zukerman, "2d arrangements," in *CGAL User and Reference Manual*, 5th ed. CGAL Editorial Board, 2020. [Online]. Available: https://doc.cgal.org/5.0.2/Manual/packages.html#PkgArrangementOnSurface2

[19] Environmental Systems Research Institute (ESRI), "Terrain, scale: 10m," 02 2020. [Online]. Available: https://www.arcgis.com/home/item.html?id=58a541efc59545e6b7137f961d7de883

[20] W. Zhang and D. R. Montgomery, "Digital elevation model grid size, landscape representation, and hydrologic simulations," *Water Resources Research*, vol. 30, no. 4, pp. 1019–1028, 1994.

[21] J. J. Maynard and M. G. Johnson, "Scale-dependency of LiDAR derived terrain attributes in quantitative soil-landscape modeling: Effects of grid resolution vs. neighborhood extent," *Geoderma*, vol. 230-231, pp. 29–40, 2014.

[22] M. T. Goodrich, "A polygonal approach to hidden-line and hidden-surface elimination," *CVGIP: Graphical Models and Image Processing*, vol. 54, no. 1, pp. 1–12, jan 1992.

[23] U. Finke and K. H. Hinrichs, "Overlaying simply connected planar subdivisions in linear time," *Proceedings of the Annual Symposium on Computational Geometry*, vol. Part F129372, pp. 119–126, 1995.

[24] J. B. Lindsay, D. R. Newman, and A. Francioni, "Scale-optimized surface roughness for topographic analysis," *Geosciences (Switzerland)*, vol. 9, no. 7, 2019.

Appendix A Terrain extents

The terrain dataset used in this project consists of the following terrains and their extents as used in the *"export raster"* tool in ArcGIS Pro [13] and the *"Terrain"* elevation layer [19]:

Name	Top	Left	Right	Bottom
AlpsBlatten	5858688	866422	878422	5844688
Andes	-2415431	-7382757	-7370757	-2429431
Andora	5248628	159122	171122	5234628
Apeldoorn	6865468	646362	658362	6851468
Appenines	5241888	1504882	1516882	5227888
Aravalli	2889538	8184562	8196562	2875538
AustralianPlains	-4042661	15475202	15487202	-4056661
Brookfield	-4063751	15524152	15536152	-4077751
CarnChuinneag	7937468	-511867	-499867	7923468
CastlePeak	4785118	-13401127	-13389127	4771118
CerroBoliv	-2500441	-7454297	-7442297	-2514441
Eikelandsosen	8472638	647792	659792	8458638
Everest	3258248	9673602	9685602	3244248
Finsteraarhorn	5875768	898332	910332	5861768
Gabriac	5498768	406162	418162	5484768
Gourdon	5433228	774402	786402	5419228
GrandCanyon	4303408	-12649207	-12637207	4289408
GWTiersTasmania	-5072921	16280862	16292862	-5086921
Hymalaya	3459318	9255762	9267762	3445318
K2	4292778	8511822	8523822	4278778
Kameuiekuuchikaushi	5265188	15888422	15900422	5251188
Karakoram	4404808	8484222	8496222	4390808
Kruger	-2884081	3533102	3545102	-2898081
KunlunChina	4453558	8499862	8511862	4439558
Liabygda	8947808	783492	795492	8933808
Lick	4566858	-8912897	-8900897	4552858
LincolnWA	6035938	-13169667	-13157667	6021938
Lowther	7454398	-422717	-410717	7440398
MaroonPeak	474330	-11916227	-11904227	4729308

Name	Top	Left	Right	Bottom
Monument	5130628	-12988007	-12976007	5116628
Moorfoot	7516658	-345897	-333897	7502658
MountFuji	4221568	15437462	15449462	4207568
MountKinabalu	682988	12969932	12981932	668988
MountWilhelm	-636581	16140522	16152522	-650581
Nebraska	5184478	-10859897	-10847897	5170478
OssaTasmania	-5142221	16236232	16248232	-5156221
Oystese	8520508	686572	698572	8506508
Paradise	5102938	-13088777	-13076777	5088938
Pyrenees	5282258	-50647	-38647	5268258
QuinnValley	5112608	-13124117	-13112117	5098608
Rocky	5506908	-12231717	-12219717	5492908
Sahara	3126578	2530192	2542192	3112578
Sairecabur	-2590661	-7562257	-7550257	-2604661
Salisbury	6678008	-216677	-204677	6664008
Serre	5552048	786782	798782	5538048
Sheep	5542608	-12177277	-12165277	5528608
SierraNegra	-85121	-10150587	-10138587	-99121
Sjani	5259368	4970502	4982502	5245368
StNiklaus	5988648	1528332	1540332	5974648
Stonehenge	6657598	-209137	-197137	6643598
Tomuraushi	5403938	15899242	15911242	5389938
Verignon	5426878	695342	707342	5412878

Appendix B Scatter plots

B.1 Single viewpoint

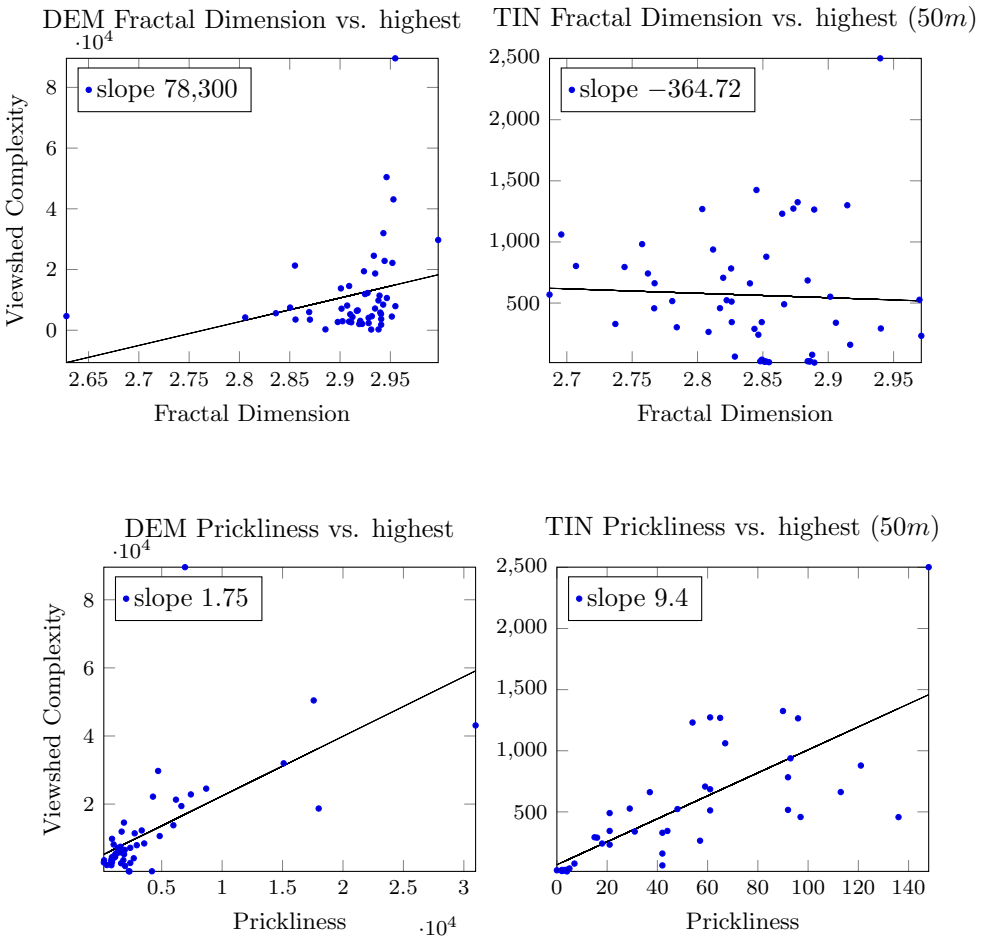

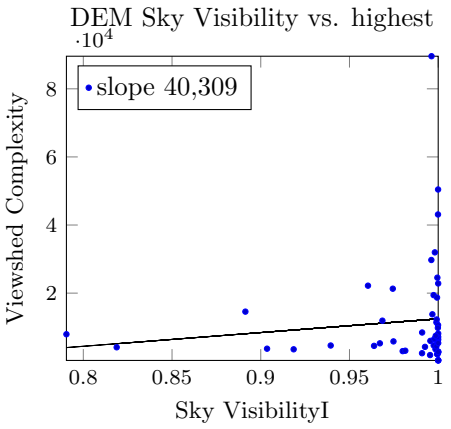
DEM Sky Visibility vs. highest
$\cdot 10^4$
slope 40,309
Viewshed Complexity
Sky VisibilityI

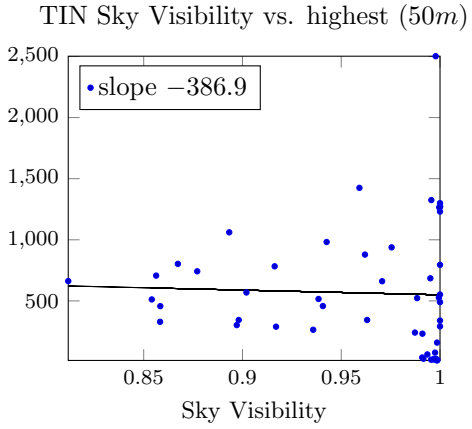
TIN Sky Visibility vs. highest ($50m$)
slope −386.9
Sky Visibility

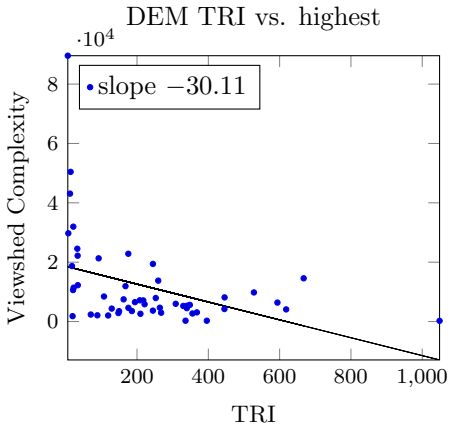
DEM TRI vs. highest
$\cdot 10^4$
slope −30.11
Viewshed Complexity
TRI

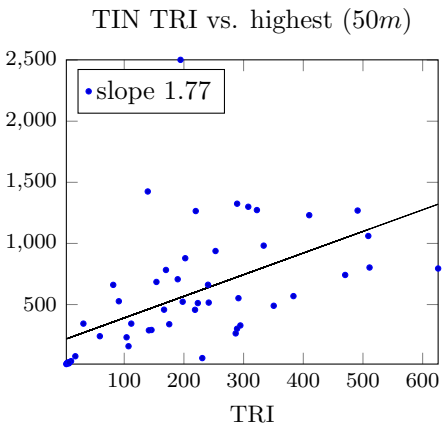
TIN TRI vs. highest ($50m$)
slope 1.77
TRI

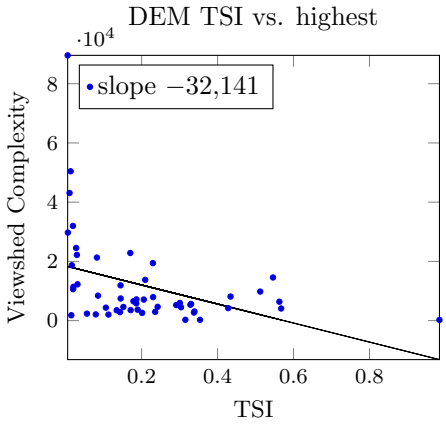
DEM TSI vs. highest
$\cdot 10^4$
slope −32,141
Viewshed Complexity
TSI

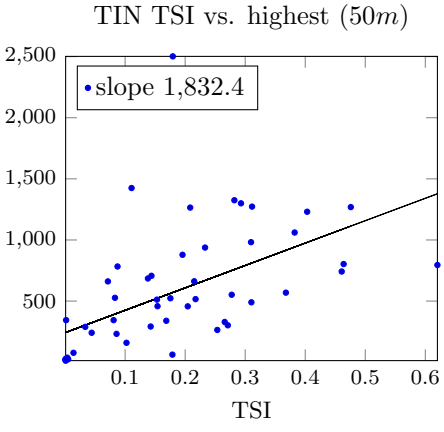
TIN TSI vs. highest ($50m$)
slope 1,832.4
TSI

DEM Fractional Dimension vs. lowest

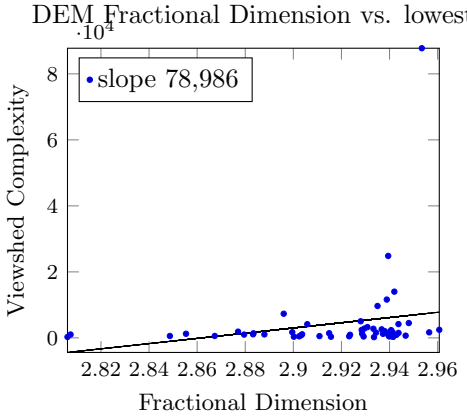

TIN Fractional Dimension vs. lowest ($100m$)

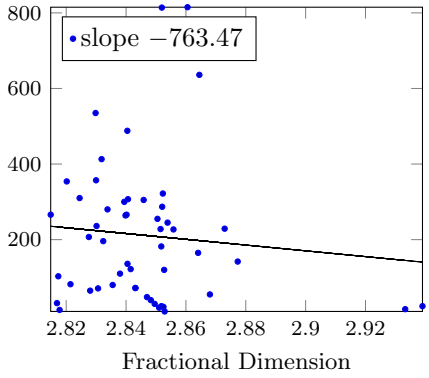

DEM Prickliness vs. lowest

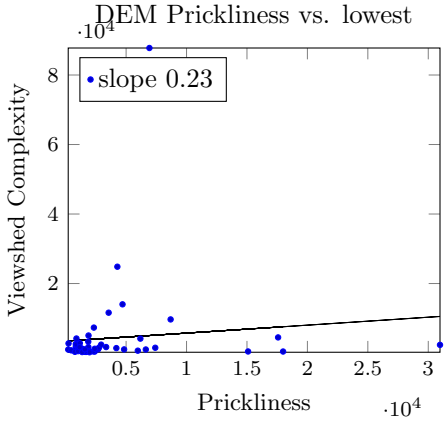

TIN Prickliness vs. lowest ($100m$)

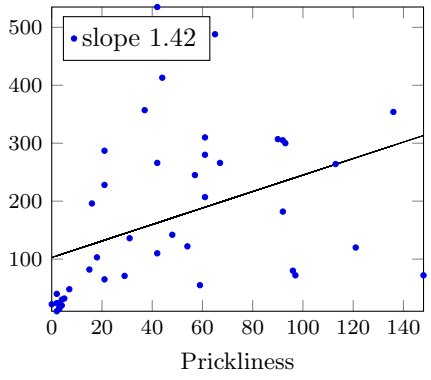

DEM Sky Visibility vs. lowest

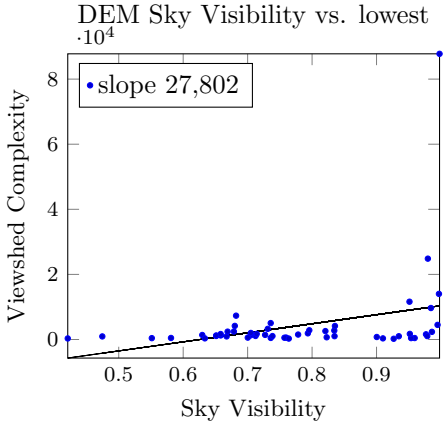

TIN Sky Visibility vs. lowest ($100m$)

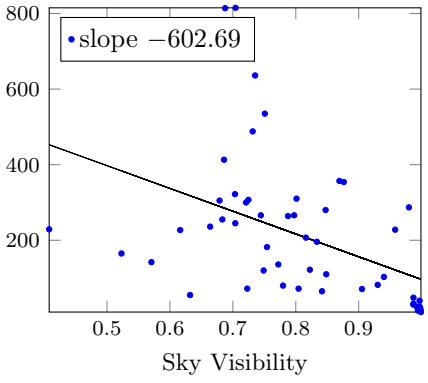

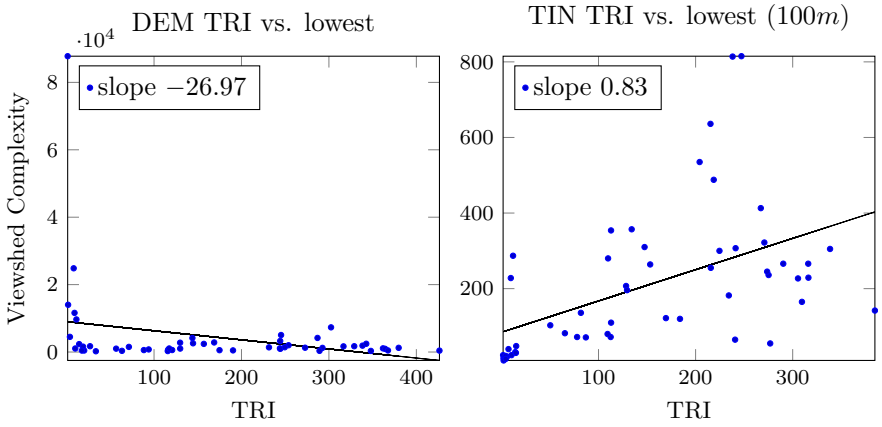
DEM TRI vs. lowest
TIN TRI vs. lowest (100m)
slope −26.97
slope 0.83
Viewshed Complexity
TRI
TRI

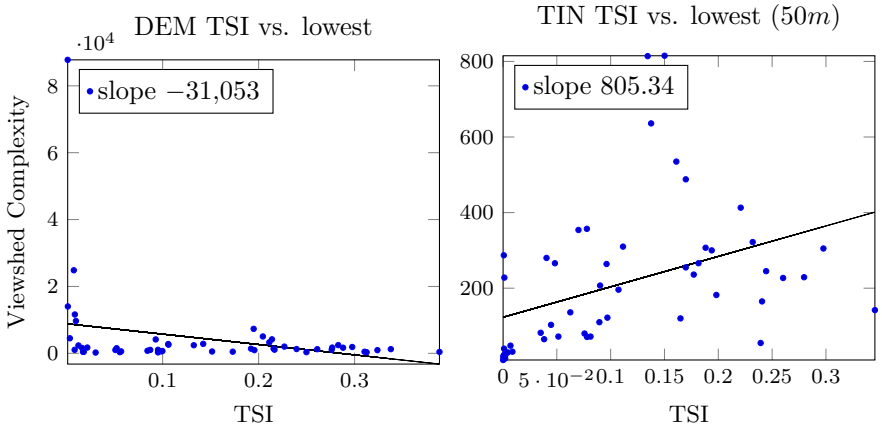
DEM TSI vs. lowest
TIN TSI vs. lowest (50m)
slope −31,053
slope 805.34
Viewshed Complexity
TSI
TSI

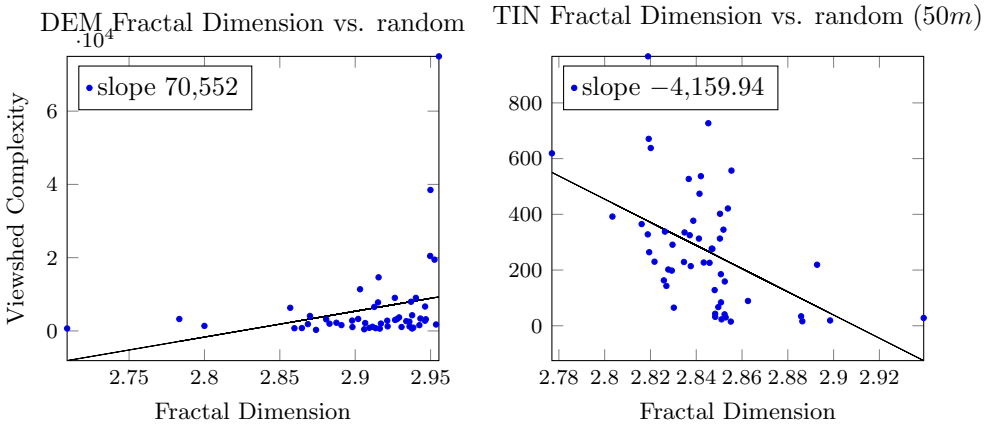
DEM Fractal Dimension vs. random
TIN Fractal Dimension vs. random (50m)
slope 70,552
slope −4,159.94
Viewshed Complexity
Fractal Dimension
Fractal Dimension

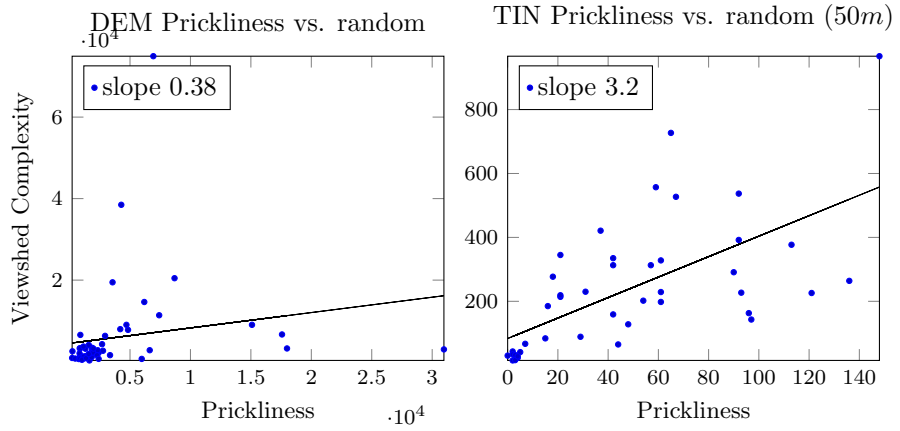
DEM Prickliness vs. random
slope 0.38
Viewshed Complexity
Prickliness
TIN Prickliness vs. random (50m)
slope 3.2
Prickliness

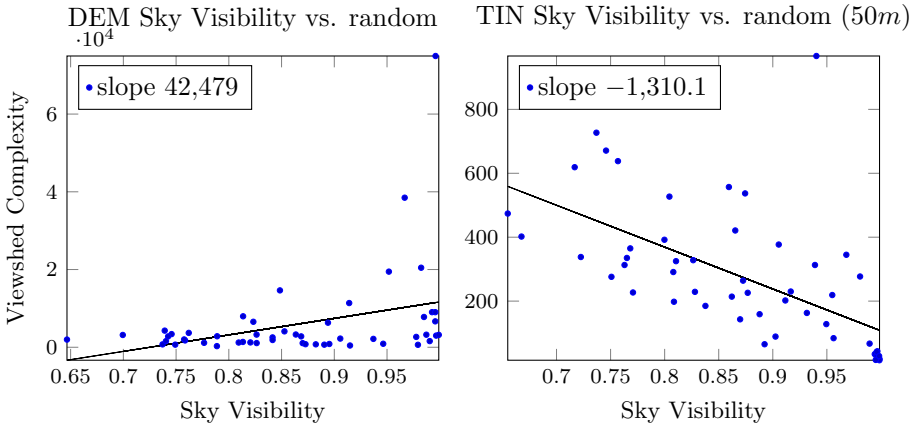
DEM Sky Visibility vs. random
slope 42,479
Viewshed Complexity
Sky Visibility
TIN Sky Visibility vs. random (50m)
slope −1,310.1
Sky Visibility

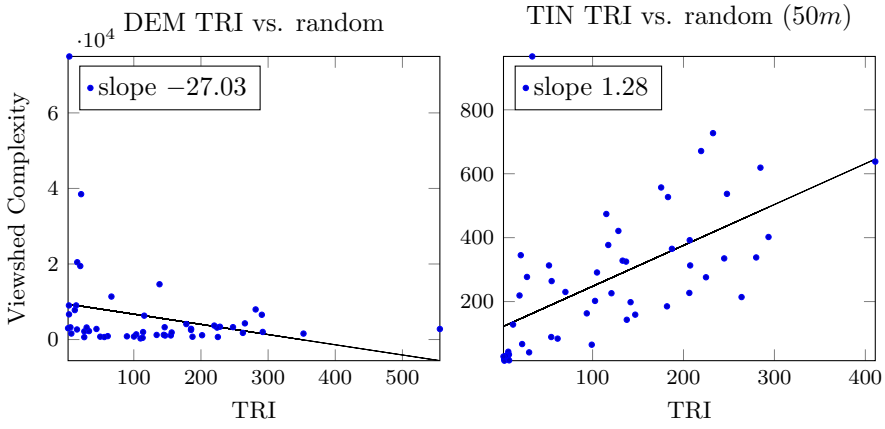
DEM TRI vs. random
slope −27.03
Viewshed Complexity
TRI
TIN TRI vs. random (50m)
slope 1.28
TRI

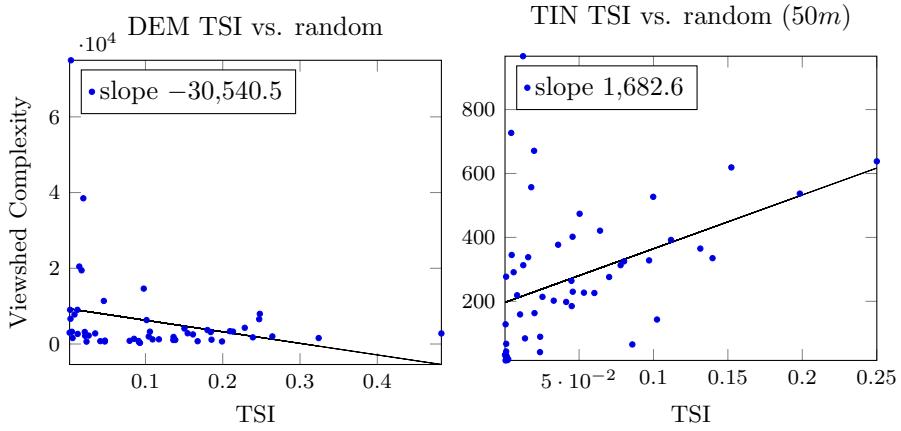

B.2 Multiple viewpoints (100m)

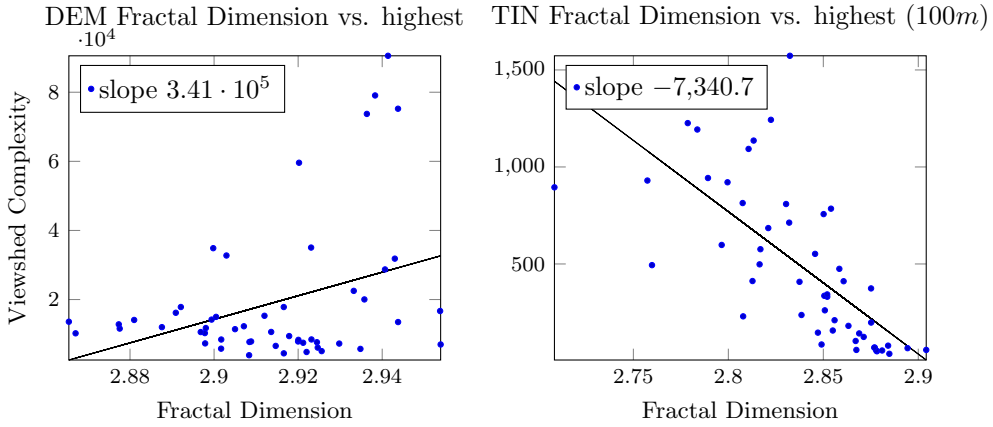

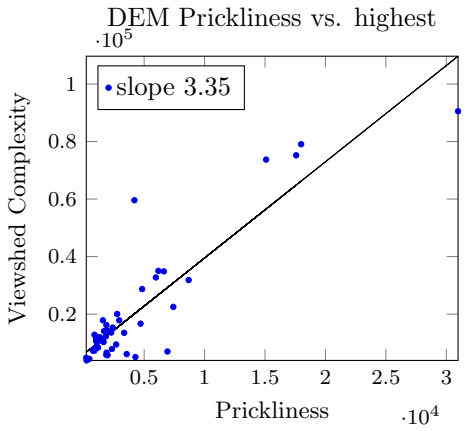
DEM Prickliness vs. highest
slope 3.35
Viewshed Complexity
Prickliness

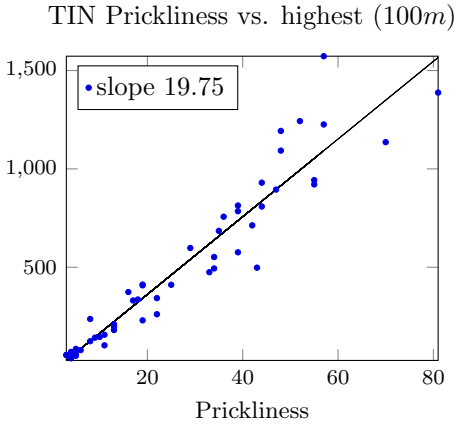
TIN Prickliness vs. highest (100m)
slope 19.75
Prickliness

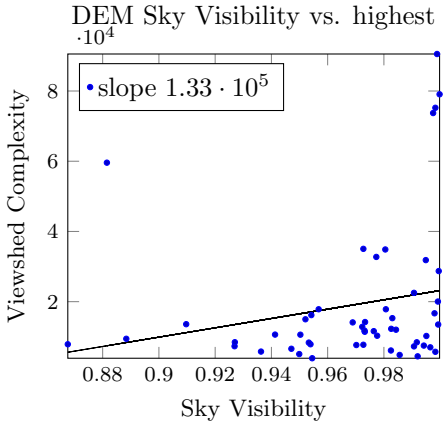
DEM Sky Visibility vs. highest
slope 1.33 · 10^5
Viewshed Complexity
Sky Visibility

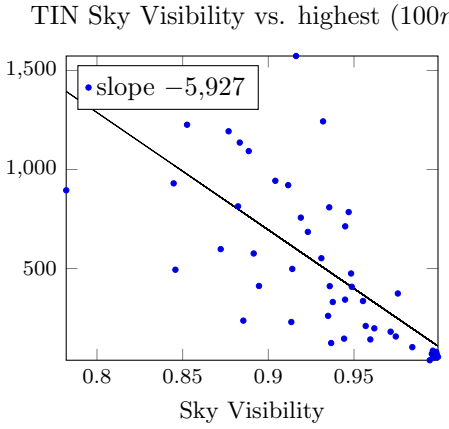
TIN Sky Visibility vs. highest (100m)
slope −5,927
Sky Visibility

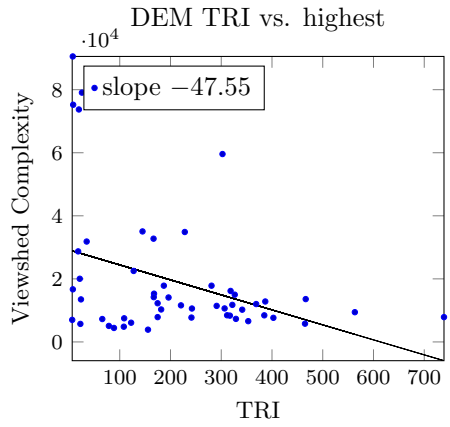
DEM TRI vs. highest
slope −47.55
Viewshed Complexity
TRI

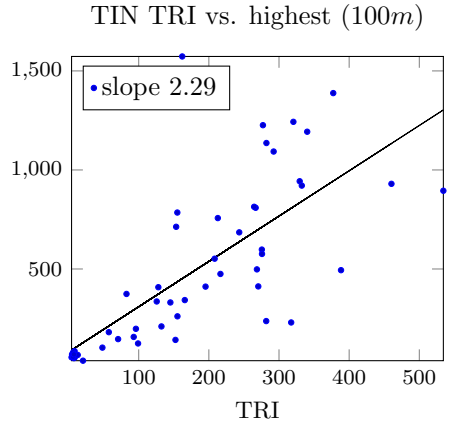
TIN TRI vs. highest (100m)
slope 2.29
TRI

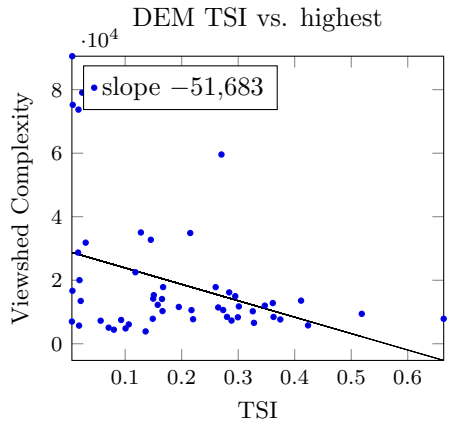
DEM TSI vs. highest
slope −51,683
Viewshed Complexity
TSI
·10^4
0
2
4
6
8
0.1
0.2
0.3
0.4
0.5
0.6

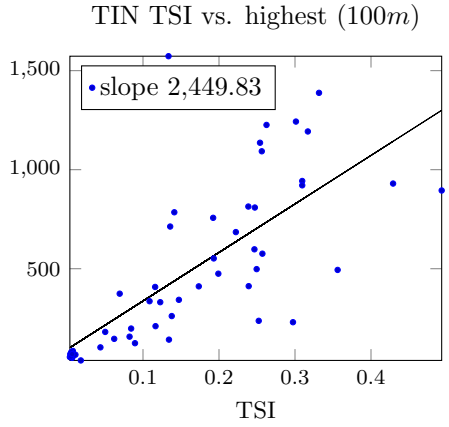
TIN TSI vs. highest (100m)
slope 2,449.83
TSI
500
1,000
1,500
0.1
0.2
0.3
0.4

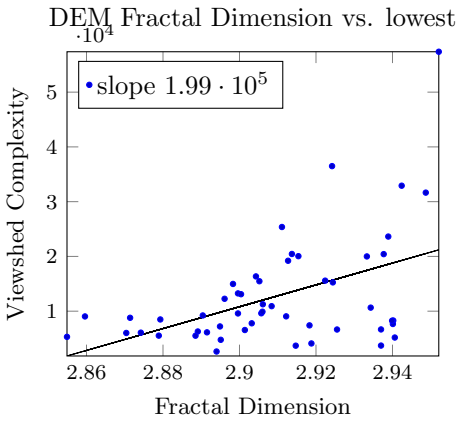
DEM Fractal Dimension vs. lowest
slope 1.99 · 10^5
Viewshed Complexity
Fractal Dimension
·10^4
1
2
3
4
5
2.86
2.88
2.9
2.92
2.94

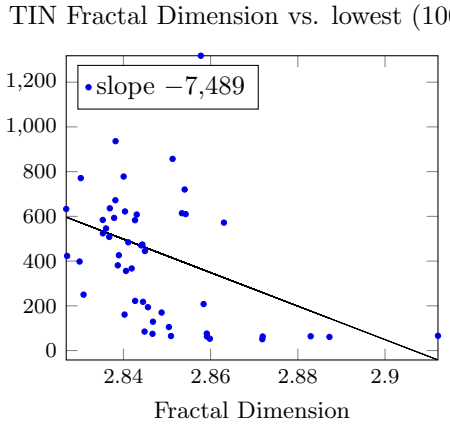
TIN Fractal Dimension vs. lowest (100m)
slope −7,489
Fractal Dimension
0
200
400
600
800
1,000
1,200
2.84
2.86
2.88
2.9

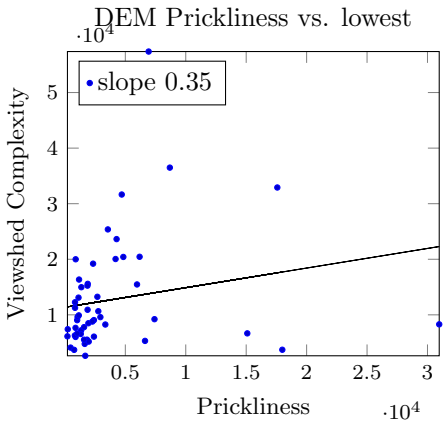
DEM Prickliness vs. lowest
slope 0.35
Viewshed Complexity
Prickliness
·10^4
·10^4
1
2
3
4
5
0.5
1
1.5
2
2.5
3

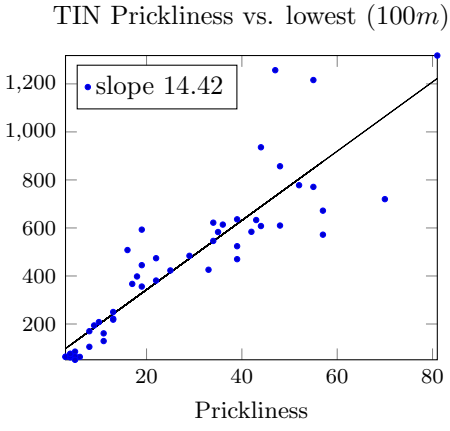
TIN Prickliness vs. lowest (100m)
slope 14.42
Prickliness
200
400
600
800
1,000
1,200
20
40
60
80

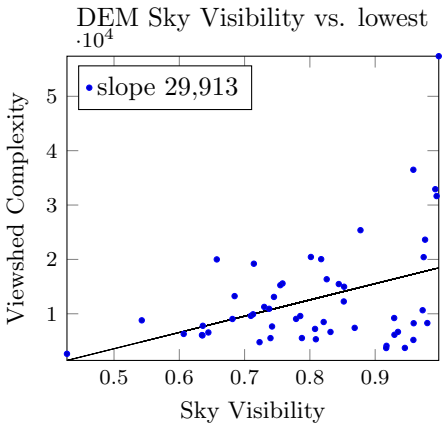
DEM Sky Visibility vs. lowest
$\cdot 10^4$
slope 29,913
Viewshed Complexity
Sky Visibility

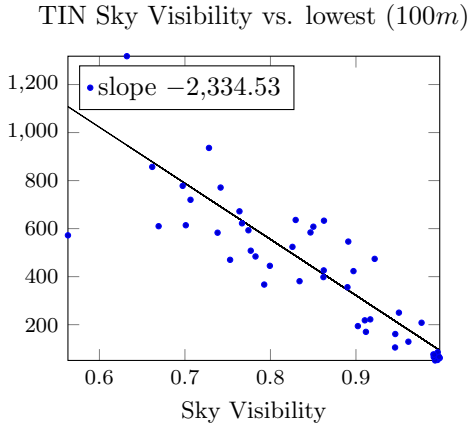
TIN Sky Visibility vs. lowest ($100m$)
slope $-2{,}334.53$
Sky Visibility

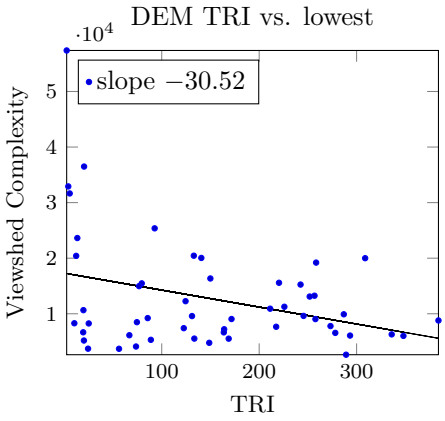
DEM TRI vs. lowest
$\cdot 10^4$
slope -30.52
Viewshed Complexity
TRI

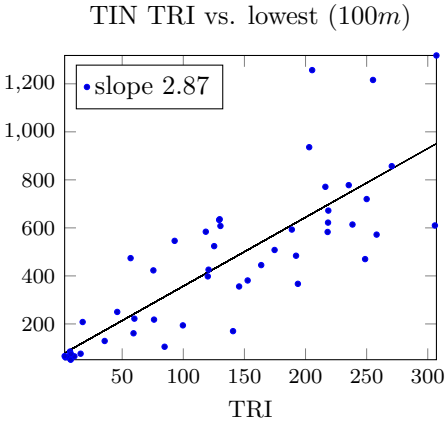
TIN TRI vs. lowest ($100m$)
slope 2.87
TRI

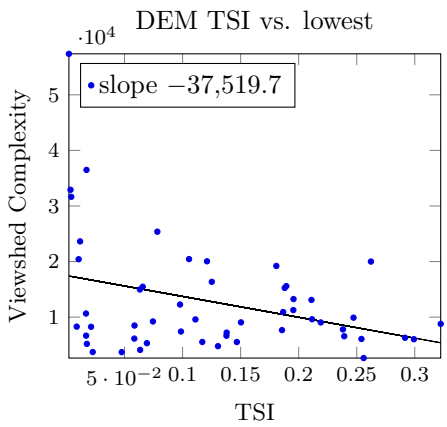
DEM TSI vs. lowest
$\cdot 10^4$
slope $-37{,}519.7$
Viewshed Complexity
TSI

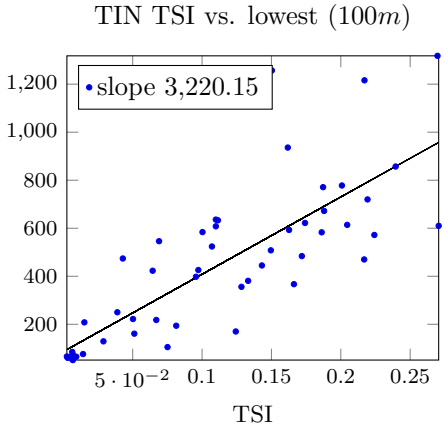
TIN TSI vs. lowest ($100m$)
slope 3,220.15
TSI

DEM Fractal Dimension vs. random

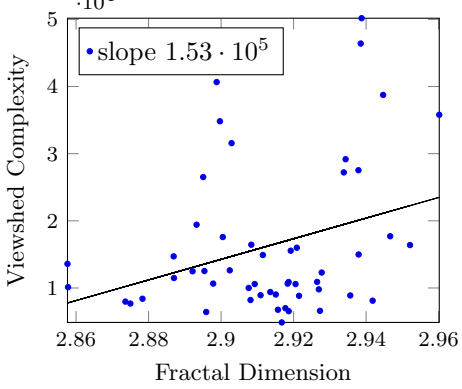

TIN Fractal Dimension vs. random ($100m$)

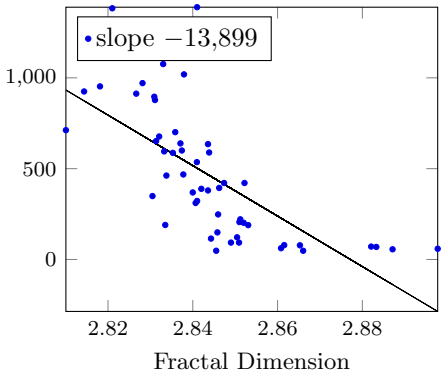

DEM Prickliness vs. random

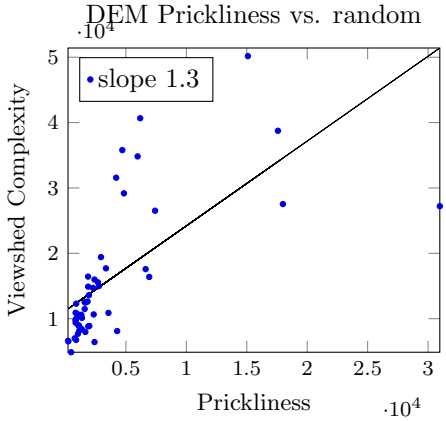

TIN Prickliness vs. random ($100m$)

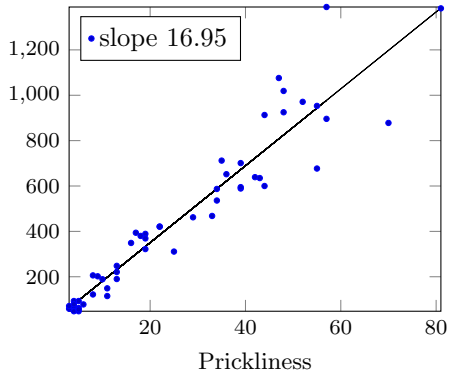

DEM Sky Visibility vs. random

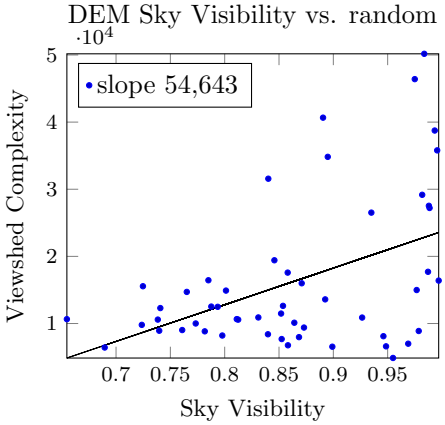

TIN Sky Visibility vs. random ($100m$)

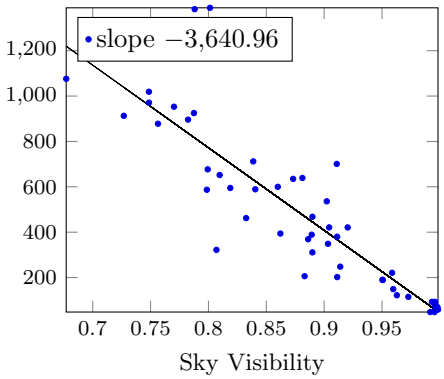

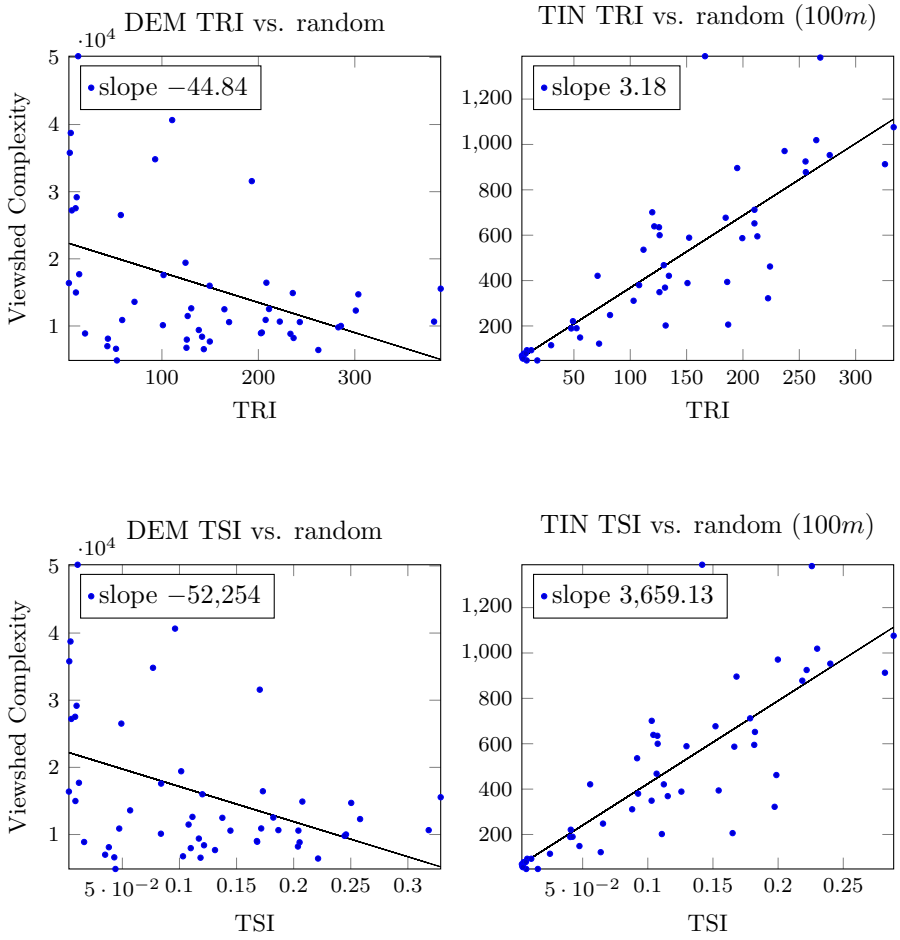
DEM TRI vs. random
TIN TRI vs. random (100m)
DEM TSI vs. random
TIN TSI vs. random (100m)
slope −44.84
slope 3.18
slope −52,254
slope 3,659.13
Viewshed Complexity
TRI
TSI
$\cdot 10^4$
$5 \cdot 10^{-2}$

B.3 Multiple viewpoints (50m)

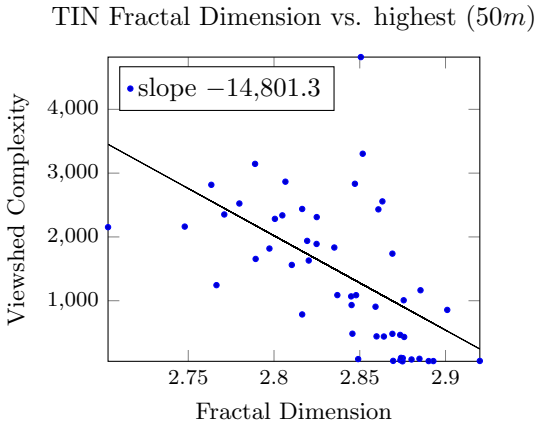

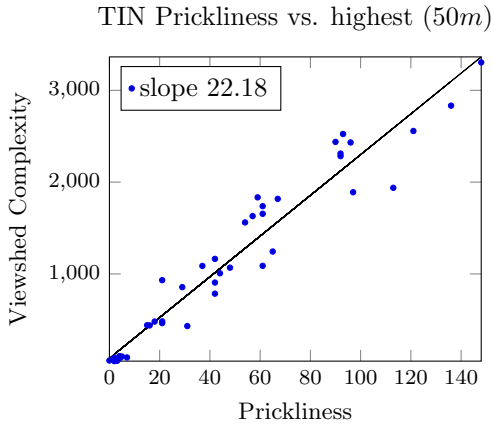

TIN Sky Visibility vs. highest ($50m$)

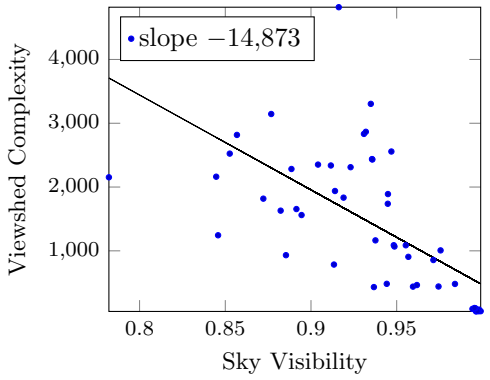

TIN TRI vs. highest ($50m$)

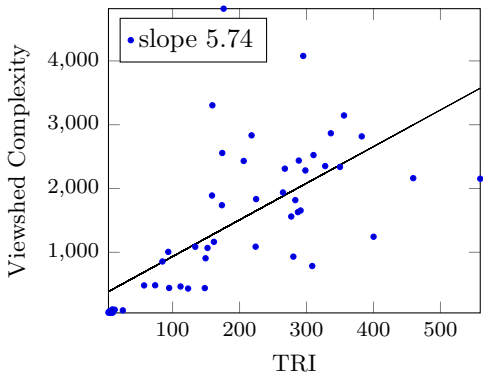

TIN TSI vs. highest ($50m$)

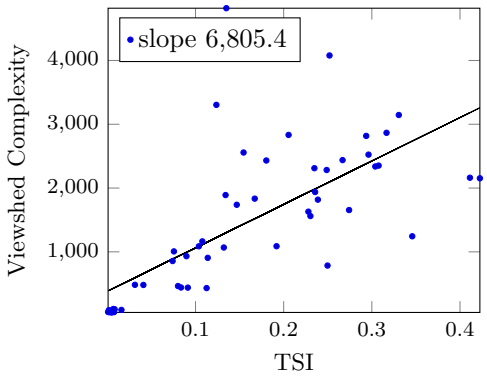

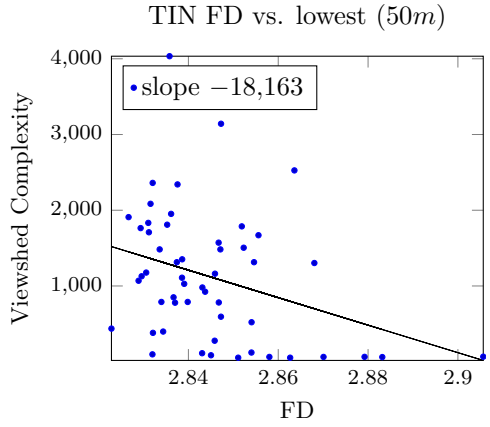
TIN FD vs. lowest (50m)
slope −18,163
Viewshed Complexity
4,000
3,000
2,000
1,000
2.84
2.86
2.88
2.9
FD

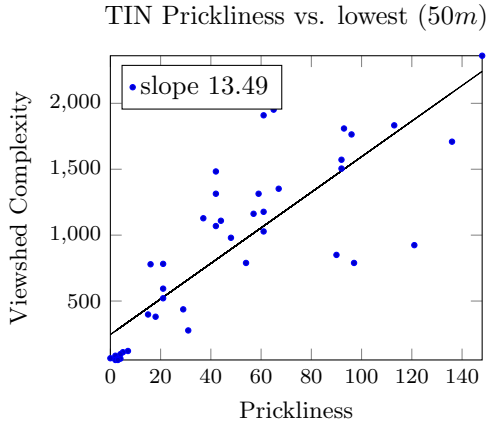
TIN Prickliness vs. lowest (50m)
slope 13.49
Viewshed Complexity
2,000
1,500
1,000
500
0
20
40
60
80
100
120
140
Prickliness

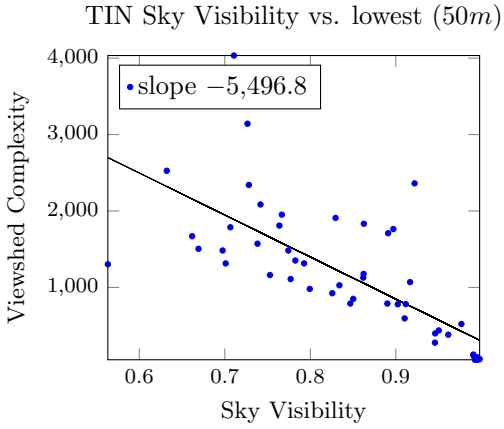
TIN Sky Visibility vs. lowest (50m)
slope −5,496.8
Viewshed Complexity
4,000
3,000
2,000
1,000
0.6
0.7
0.8
0.9
Sky Visibility

TIN TRI vs. lowest ($50m$)

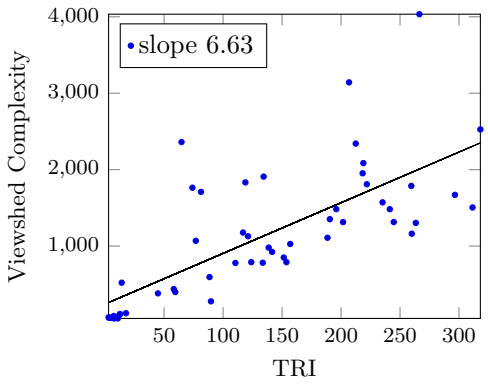

TIN TSI vs. lowest ($50m$)

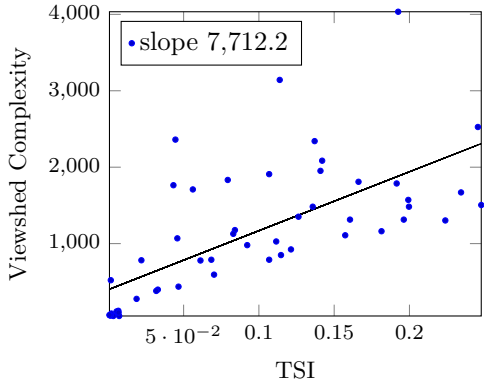

TIN Fractal Dimension vs. random ($50m$)

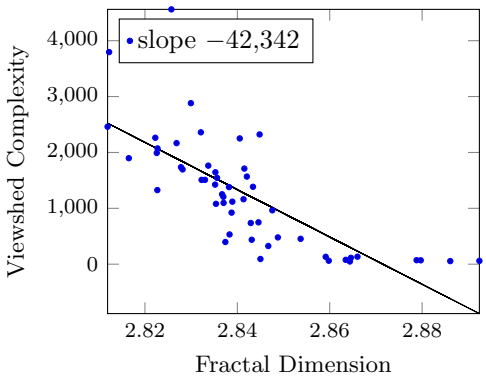

TIN Prickliness vs. random ($50m$)

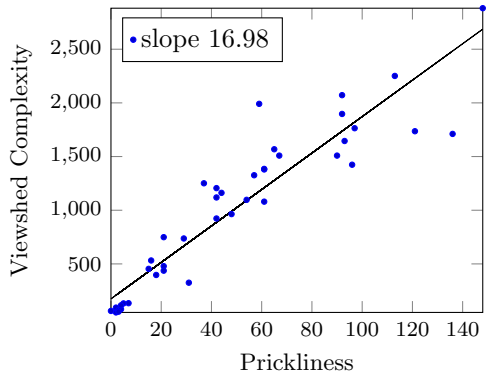

TIN Sky Visibility vs. random ($50m$)

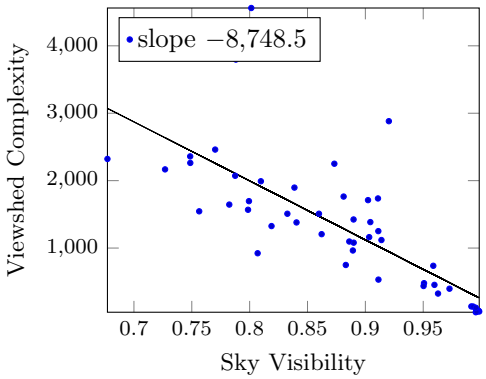

TIN TRI vs. random ($50m$)

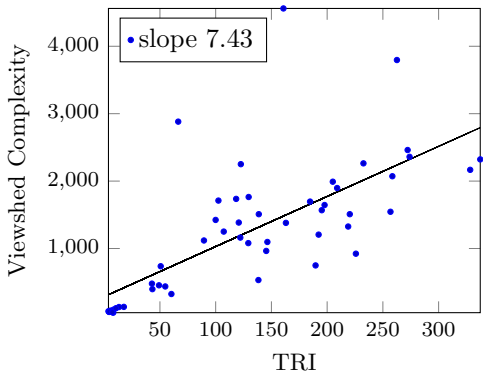

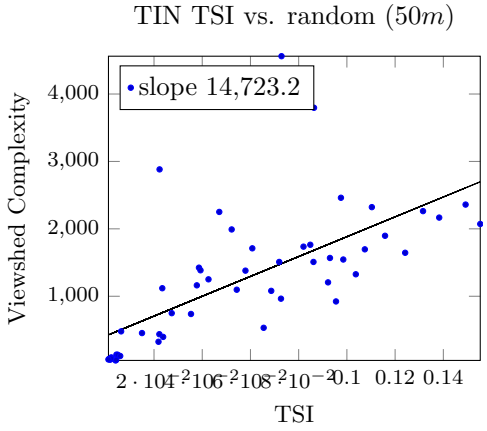
TIN TSI vs. random ($50m$)
slope 14,723.2
Viewshed Complexity
4,000
3,000
2,000
1,000
$2 \cdot 10^{-2}$
$4 \cdot 10^{-2}$
$6 \cdot 10^{-2}$
$8 \cdot 10^{-2}$
10^{-2}
0.1
0.12
0.14
TSI